EUROPEAN ORGANIZATION FOR NUCLEAR RESEARCH

CERN-EP/79-117
8 October 1979

AN EXPERIMENTAL TEST OF EXCHANGE DEGENERACY IN THE REACTIONS $\pi^+p\to K^+\Sigma^+$, $\pi^+p\to K^+\Sigma^+(1385)$ AND THEIR LINE REVERSED PARTNERS.

A. Berglund[1(6)], T. Buran[2(7)], P.J. Carlson[1],
C.J.S. Damerell[3], I. Endo[2(8)], A.R. Gillman[3],
V. Gracco[4], R.J. Homer[5], M.J. Hotchkiss[3],
A. Lundby[2], M. Macri[4], B.N. Ratcliff[3(9)],
A. Santroni[4], T. Tso[3(10)], F. Wickens[3], J.A. Wilson[5]

ABSTRACT

A description is given of an experimental study of Exchange Degeneracy (EXD) in hypercharge exchange reactions using the line reversed partners $\pi^+p\to K^+\Sigma^+$ ($K^-p\to\pi^-\Sigma^+$) and $\pi^+p\to K^+\Sigma^+(1385)$ ($K^-p\to\pi^-\Sigma^+(1385)$) at incident momenta of 7.0 and 10.1 GeV/c. Both pairs of reactions were measured in the same apparatus, with particular care being taken to minimize relative normalization errors. For the Σ production reactions we present high statistics measurements of the differential cross-sections and polarizations from $t'=0$ to large t. The general trends of the data agree with naive expectations from weak EXD. The cross-section difference in the extreme forward direction at the higher momentum is consistent with zero and there is a general reduction in the cross-section differences going from the lower to the higher momentum. The polarizations are approximately equal in magnitude and of opposite sign between the two reactions. On the other hand, the data do not agree with the detailed predictions of EXD. The slope for the positive reaction is systematically steeper in the forward region than for the negative reaction and there is a complex s and t dependence for the cross-section differences including a cross-over at $t \simeq -0.8$ $(GeV/c)^2$. For the $\Sigma(1385)$ production reactions, we present differential cross-section measurements in the forward region ($|t|<0.3$ $(GeV/c)^2$). The cross-section differences are substantial and essentially constant over the s and t ranges studied.

(Submitted to Nuclear Physics)

[1] University of Stockholm, Sweden
[2] CERN, Geneva, Switzerland
[3] Rutherford Laboratory, Chilton, Didcot, Oxon, England
[4] Instituto di Fisica dell'Università, INFN, Sezione di Genova, Italy
[5] Physics Department, University of Birmingham, England
[6] Present address: CERN, Geneva, Switzerland
[7] Present adress: University of Oslo, Norway
[8] Present address: Physics Department, University of Hiroshima, Japan
[9] Present address: SLAC, USA
[10] Present address: Brookhaven National Laboratory, USA

1. INTRODUCTION

The absence of exotic two body states (e.g. $K^+\pi^+$) and the concept of duality in particle reactions, produces the attractive idea of exchange degeneracy for Regge trajectories [1].

This model leads to simple predictions for the behaviour of various reactions. For example, according to Regge pole ideas, at high energies the hypercharge exchange reaction

$$\pi^+p\rightarrow K^+\Sigma^+ \quad (1)$$

should be dominated by the exchange of the K* and K** trajectories. If these are exchange degenerate (identical trajectory functions $\alpha_{K^*}(t)=\alpha_{K^{**}}(t)$) then this reaction and its line reversed partner

$$K^-p\rightarrow\pi^-\Sigma^+ \quad (2)$$

should have equal differential cross-sections and polarizations of equal magnitude but of opposite sign (weak exchange degeneracy). If in addition the residues for the amplitudes are equal then the cross sections are again the same but now the polarizations should be zero (strong exchange degeneracy).

Similar remarks apply to the line reversed processes where $\Sigma(1385)$ replaces $\Sigma(1190)$.

$$\pi^+p\rightarrow K^+\Sigma^+(1385) \quad (3)$$
$$K^-p\rightarrow\pi^-\Sigma^+(1385) \quad (4)$$

and also to the KN charge exchange reactions which involve the exchange of the ρ and A_2 trajectories (see for example [2]).

Prior to this experiment, the prediction of equal cross-sections was poorly tested in both pairs of hypercharge exchange reactions, because of the difficulty in comparing independent experiments with large normalization uncertainties. The predictions for the polarization were untested because no measurements of the polarization in reaction (2) had been made above 5 GeV/c.

This paper presents the final results from the first experiment to study these line reversed partners in the same apparatus. Some of the results have been presented in earlier publications [3,4,5,6]. Section 2 contains details of the experimental setup. Section 3 describes the data analysis, gives details about the program used to calculate the geometrical acceptances, and also discusses the corrections necessary for determining the absolute cross-sections. In section 4 the results are presented together with some comparisons and discussions concerning the s and t dependences of the data. We have also tried to summarize the theoretical progress that has been made towards understanding the features of hypercharge exchange processes. Finally, in section 5 we state our conclusions.

2. EXPERIMENTAL SETUP

2.1 GENERAL FEATURES

The experiment, which will be described in some detail in this section, was performed, using counter and spark chamber techniques, in a high momentum beam from the CERN PS. Two different layouts of the apparatus were used.

The first arrangement (geometry 1) was used at 10.1 GeV/c only, for measurements in the low $|t|$ region[1]. The non-interacting beam passed through the active areas of the detectors, giving 100% acceptance at small scattering angles. In geometry 1 no recoil detector was included (i.e. only the forward mesons were detected). This single arm setup was appropriate because slow Σ^+'s produce decay products with large angular and energy spreads and are consequently difficult to detect reliably.

In the second arrangement (geometry 2), which was used at 10.1 and 7.0 GeV/c, a recoil arm was added to detect the charged products from the Σ^+ decay. This layout covered a larger t range than geometry 1 and enabled the polarizations for reactions (1) and (2) to be measured by using the known large asymmetry parameter for the decay $\Sigma^+ \to p\pi^0$.

2.2 INCIDENT BEAM

The downstream section of the incident (unseparated) beam is shown in fig. 1. Beam particles were identified by a set of scintillators 1BS, 2BS, 3BS, a halo counter 1BA, and three threshold Cerenkov counters BC1, BC2, and BC3. For each event a pulse height measurement was recorded for each of these detectors. The position of the incident particle was measured by four counter hodoscopes H1 and H2 (5 mm wide elements measuring X and Y) and H3 and H4 (3 mm wide elements measuring X and Y). The separation between H1/2 and H3/4 was 7.5 m. An array of scintillators (p-hodo) placed at a momentum dispersed focus measured the incident momentum. These elements were calibrated by using the forward particle spectrometer to measure the momenta of the non-interacting beam particles.

An incident particle was defined by the coincidence requirement $1BS.2BS.3BS.(\overline{1BA})$. For the 10.1 GeV/c measurements the beam Cerenkov counters were set to detect particles as follows:

(1) positive beam - BC1 (π+K), BC2 (π+K) and BC3 (π)
(2) negative beam - BC1 (π), BC2 (π+K) and BC3 (π)

For both polarities at 7.0 GeV/c the identification was as follows:

BC1 (π), BC2 (π+K) and BC3 (π)

---

[1]Throughout this paper we use the Mandelstam variables $t=(p_1-p_3)^2$ and $s=(p_1+p_2)^2$, where p_1 and p_2 are the 4-momenta of the incident meson and proton and p_3 that of the outgoing meson. We also use $t'=t-t_{min}$.

The beam fractions at 7.0 GeV/c and 10.1 GeV/c are given in table 1. In addition the μ/π and e/π fractions were 3% and <0.1% respectively.

2.3 GEOMETRY 1

As already described in 2.1 this layout, which is shown in fig. 2 was used at 10.1 GeV/c for small four-momentum transfer measurements ($|t| < 0.3$ (GeV/c)^2). Basically the apparatus consisted of a single arm spectrometer, measuring the scattering angle and momentum of identified forward going particles, which emerged from the 100 cm long liquid hydrogen target. The magnetic field integral for a trajectory was typically 3.3 Tm.

2.3.1 Trigger counters

Three arrays of scintillation counters were used in triggering the apparatus. The first array, T_1 (5 elements each 10 cm wide and 30 cm high), detected charged particles entering the spectrometer. Multiple hits were accepted from this array thus allowing for the possibility of extra hits from δ-rays, interaction products, and accidental tracks.

The second array, T_2 (13 elements - 11 of 10 cm, 1 of 12 cm and 1 of 16 cm - all 60 cm high) detected charged particles after the magnets. Here only single hits were allowed in the trigger.

The final array T_5 (5 elements each 30 cm wide and 76 cm high) was placed behind 1.8 m of iron and was used in anti-coincidence. Its main purpose was with the negative beam where it was used to eliminate the large event rate due to muons from $K\mu_2$ decay (kinematically similar to reaction (2)).

2.3.2 Cerenkov detectors

Good particle identification was achieved by including three threshold Cerenkov counters C_0, C_1, and C_2 in the spectrometer: the thresholds were set to detect the following particles with momenta similar to the beam momentum.

Positive beam - C_0 (π), C_1 (π+K), and C_2 (π)
Negative beam - C_0 (π), C_1 (π), and C_2 (π)

The first Cerenkov counter, C_0, was a 1 m long cylinder 50 cm in diameter, filled with Freon 12 at atmospheric pressure, and viewed from the side (using a 45^0 inclined mirror) with a 5" diameter photomultiplier (RCA 4522). This counter was used in anti-coincidence for reaction (1) because it was able to detect and eliminate non-interacting beam pions immediately after the target. These could interact further downstream (e.g. in C_1, T_2, etc.) and satisfy the downstream logic, thus producing a potentially high trigger rate. C_0 was not used in the trigger for reaction (2).

For reaction (1) the kaon was identified using C_1, a pressurized counter filled with Freon 13. A spherical mirror focussed the light

through a 10 cm thick fused silica window onto a close-packed array of seven 5" diameter photomultipliers (RCA 8854). This counter was designed to have a good angular acceptance (±20° horizontally and ±4.5° vertically) and high light collecting efficiency. To demonstrate its performance fig. 3 shows the pulse height distribution for 10 GeV/c kaons.

The final Cerenkov counter in the spectrometer was C_2, an atmospheric pressure counter filled with Freon 12 which had a minimum radiator length of about 250 cm. The mirror plane consisted of two rows of seven mirrors (total area 350 x 120 cm²). These mirrors focussed the light into light collectors [7] attached to 5" diameter photomultipliers (RCA 4522). Again good angular acceptance and light collection efficiency was achieved in the design. Fig. 4 shows the pulse height distribution obtained for 10 GeV/c pions.

2.3.3 Spark chambers and read-out

Particle trajectories through the spectrometer were measured using five modules of wire spark chambers, W_1 - W_2, W_4 - W_6, with 1 mm spacing between the wires. Each module contained two 10 mm gaps and all four wire planes were read, thus providing four co-ordinates per module. The chambers were of three different sizes: W_1 and W_2 had active areas of 110 x 30 cm² (horizontal x vertical); W_4 and W_5 had areas of 230 x 60 cm², and W_6 was 200 x 100 cm². The wires were inclined to the vertical as follows: 15, -15, 0 and -30 degrees for W_1 - W_5 and 15, -15, 15, and -15 degrees for W_6 (the two gaps of W_6 were tilted by ±3 degrees to the horizontal to help in resolving ambiguities).

Each wire in a plane was connected to a 6800 pF capacitor, a diode and a sense line. Wires were addressed in groups of 32. Normally the capacitor was in a discharged state but during a spark it was charged up through diodes. Capacitors on the low voltage plane were charged negatively, and those on the high voltage plane were charged positively. At read-out time the capacitors were discharged through the sense lines [8]. When the chambers were read a signal was applied to each address line in turn and the sense signal was combined with the address by the read-out electronics to give the wire number. The electronics also combined consecutive signals to form clusters and the final output was a series of 16 bit words containing the necessary coded information.

Two parallel read-out units were used, each accessing 1500 addresses with 3 μs needed for each address. An additional 3μs per cluster was necessary to sort adjacent hits into N clusters (N typically 30). Finally the addresses were cleared after each event (a second 'read'). Thus the total time required to read out the event was

$$T = 9.0 \text{ ms} + 3N\ \mu\text{s} \quad \text{(typically 9.1 ms)}$$

which represented the overall event dead time, since the spark chambers pulsing system had fully recovered within this period.

2.4 GEOMETRY 2

The second geometry adopted in the experiment is shown in fig. 5. This differed from geometry 1 in that the beam passed outside the active areas of the spark chambers. This permitted the use of high beam intensities (3.10^6 s^{-1}) and enabled cross-section measurements to be made out to large $|t|$ values (about 2 $(GeV/c)^2$)). For events satisfying the low $|t|$ cutoff of the forward arm, the recoil Σ's from the hypercharge exchange reactions have sufficient momentum to allow efficient detection of the decay protons (in the case of $\Sigma^+ \rightarrow p\pi^0$). Thus for this geometry, a recoil detection arm was added.

2.4.1 Modifications from geometry 1

Many features of this geometry are similar to those described in 2.3. Only the significant changes will be discussed.

A second large wire spark chamber module, W_7, (again tilted with respect to the horizontal) was added to complement W_6, and the trigger arrays T_1 and T_2 were enlarged (T_1 now had 8 elements of 10 cm width and T_2 was extended by adding 2 of 16 cm and 3 of 20 cm width).

An additional triggering array T_4 (covering 260 x 103 cm^2) was added to ensure that the particles traversed the entire spectrometer, since for reaction (1) a significant trigger rate was caused by small angle particles missing the spark chambers but interacting in the T_2 light guides.

The iron filter and the small upstream Cerenkov counter C_0 were removed and a scintillation counter, 2BA, was added downstream of the target to veto the non-interacting beam particles (the role C_0 had fulfilled in geometry 1).

Forward scattered particles were deflected in the opposite sense to that for geometry 1 and this involved some small movements of the forward detectors with respect to the magnets.

2.4.2 Recoil arm

To detect the recoil particles a second arm was added to the apparatus, consisting of three modules of wire spark chambers, W_8 - W_{10}, and a scintillation counter array T_3.

The spark chambers were identical to W_6 and W_7, with the two gaps of each module angled by +7 and -8 degrees to the horizontal plane to help in resolving ambiguous co-ordinates. The details of the read-out are as described in 2.3.3.

The counter array T_3 consisted of two layers of scintillator with a 10 mm thick sheet of aluminium between them. Front-back coincidences were required between corresponding elements. Each layer of scintillator contained eight elements (30 cm wide and 76 cm high). The aluminium was needed to reduce the possibility of triggering on a forward particle with a δ-ray in the recoil arm.

An array of anti-coincidence counters, TA, surrounded the target and covered the solid angle not seen by the forward or recoil arms. These were also sandwich type counters with 3 mm of aluminium between two layers of scintillator. Requiring front-back coincidences between corresponding elements avoided the loss of events accompanied by δ-rays, but allowed the rejection of events with extra charged hadrons.

2.5 EVENT TRIGGERING AND RATES

2.5.1 Geometry 1 at 10.1 GeV/c

The triggering requirement for this geometry and the corresponding rates were as follows:

$\pi^+p\rightarrow K^+\Sigma^+$	$\pi_b.T_1.T_2(=1).(\overline{C_0}).C_1.(\overline{C_2})$	Rate 18 per 10^4 π_b
$K^-p\rightarrow \pi^-\Sigma^+$	$K_b.T_1.T_2(=1).(\overline{T_5}).C_1.C_2$	Rate 220 per 10^4 K_b

where π_b and K_b indicate an incident pion or kaon (the second rate is much higher than the first because of $K\pi_2$ decays).

Because the non-interacting beam traversed the active region of the spectrometer the data were collected with a total beam intensity limited to 3.10^5 s^{-1}, giving typically 20 events per pulse.

In addition to these events the apparatus was triggered on scaled down rates of incident pions and kaons for both beam polarities, the scaling factor being chosen to give about one pion and one kaon event per pulse. This feature enabled empirical corrections to be made for losses in the apparatus (see section 3.4), and provided a precise determination of the incident beam profile, for use in the acceptance Monte Carlo calculation.

In order to eliminate accidental tracks in the chambers any event which was preceeded or followed by another beam particle within the sensitive time of the spark chambers was rejected.

2.5.2 Geometry 2 at 10.1 GeV/c

The triggering requirement and the corresponding rates for this geometry were as follows:

$\pi^+p\rightarrow K^+\Sigma^+$ $\quad \pi_b.(\overline{2BA}).T_1.T_2(=1).T_3.(\overline{TA}).T_4.C_1.(\overline{C_2})$
Rate 2 per 10^4 π_b

$K^-p\rightarrow \pi^-\Sigma^+$ $\quad K_b.(\overline{2BA}).T_1.T_2(=1).T_3.(\overline{TA}).C_1.C_2$
Rate 4 per 10^4 K_b

The introduction of the side arm requirement and vetoing of very small $|t|$ particles decreased the trigger rate for the first process by about a factor of 10, and eliminated all the kaon decay backgrounds for the second one, giving a reduction in trigger rate by a factor of about 50.

The total beam intensity used for this phase of the experiment was 3.10^6 s^{-1}, and typical trigger rates were 10-20 events per pulse for the first reaction and 5 per pulse for the second.

As for geometry 1, beam particle events were accepted at a low rate for calibrations.

Since the trigger rate for the second reaction was low, elastic scattering triggers were included for the minority particles (e.g. K^- and $\bar{p}$). These events are the subject of a subsequent paper [9]. As well as these event types a single arm annihilation trigger was included ($\bar{p}p \to \pi^+ X$, [6]).

2.5.3 Geometry 2 at 7 GeV/c

In order to study the s dependence of the cross-sections the experiment was repeated at 7.0 GeV/c with the same apparatus as already described in section 2.4. For both processes a simple forward arm trigger was included to enable direct comparisons to be made with the 10.1 GeV/c geometry 1 results. This had, in contrast to the 10.1 GeV/c results, a low $|t|$ cut-off.

The trigger requirements and rates were as follows:

$\pi^+p \to K^+\Sigma^+$ 2 arm As in 2.5.2
Rate 2 per 10^4 π_b

1 arm $\pi_b.(2BA).T_1.T_2(=1).T_4.C_1.(C_2)$
Rate 12 per 10^4 π_b

$K^-p \to \pi^-\Sigma^+$ 2 arm As in 2.5.2
Rate 2 per 10^4 K_b

1 arm $K_b.(2BA).T_1.T_2(=1).T_4.C_1.C_2$
Rate 8 per 10^4 K_b

The 2 arm rates are very similar to the 10.1 GeV/c geometry 2 rates, and the 1 arm rates are much lower than the geometry 1 rates at 10.1 GeV/c, the beam associated backgrounds having been essentially eliminated.

For this phase of the experiment the total flux was 3.10^6 s^{-1}. It was therefore necessary to disable the 1 arm events on most data runs with the positive beam since they saturated the triggering. Beam particles were as usual taken for calibrations.

3. DATA ANALYSIS

The analysis was performed in several steps. First, for the particles in the forward spectrometer, tracks were found and the momentum and the missing mass were calculated. Plots of typical raw missing mass distributions for a small sample of the data are shown in fig. 6, and indicate a large background below the Σ and $\Sigma(1385)$ peaks.

The second step was to impose cuts on a number of measured quantities for the event (pulse heights in Cerenkov counters etc.) which proved extremely effective in reducing the background to a low level.

For the 2-arm data a further step was used to find the trajectory of the corresponding recoil particle in the side arm. This step served to define a clean fiducial volume for recoil particles, to impose further kinematic constraints and to provide information on the polarization.

3.1 TRACK FINDING

The track finding in the forward spectrometer was comparatively simple, because in general there was only a single track with a few extra sparks. Tracks were first found in the spark chambers downstream of the magnets, where extra sparks and any additional tracks were unlikely to cause confusion. These downstream tracks were then used as constraints in the fitting of the upstream tracks, where the track finding was more easily confused, due to the limited separation of sparks. The upstream and downstream tracks were then used to determine the momentum of the forward particle, in such a way as to minimize the effect of the multiple scattering in the high pressure Cerenkov counter C_1.

The track finding in the side arm chambers was complicated by the presence of hadron showers produced in beam line magnets upstream of the target from a low momentum tail of the beam, giving high multiplicities of unwanted tracks. We therefore limited the side-arm track finding to events where the forward arm particle satisfied the cuts for a specific reaction (e.g. elastic scattering, $\pi^+p\rightarrow K^+\Sigma^+$ etc.) and to the region of the side-arm chambers defined by the hit T_3 counter and the primary vertex, allowing for the vertex uncertainty and the decay of the Σ^+. This procedure gave a good efficiency for finding the genuine recoil trajectory, and for rejecting the background tracks.

3.2 BACKGROUNDS AND CUTS

The most serious background affecting the single arm data at 10 GeV/c came from the misidentification of the incident beam particle. For example, an incident K^+ misidentified as a π^+ (say by production of a δ electron in BC3) would then be a good candidate to make a hypercharge exchange trigger since it would satisfy the Cerenkov requirement in the forward spectrometer. There were various causes for such a misidentification (including double beam tracks within the resolving time of the beam logic). All of these could be removed with high efficiency by using pulse height cuts on the signals from the incident beam Cerenkov and scintillation counters. For example, fig. 7 shows scatter plots of the pulse heights in two of the beam Cerenkov counters for the case of an incident pion trigger, and for the $\pi^+p\rightarrow K^+$(Missing mass) trigger. For the second trigger it can clearly be seen that BC3, set to count pions only, was detecting a large number of particles with very low pulse heights. The distribution in the other Cerenkov counters show that these were kaons. These misidentified kaons contributed 53% of all triggers in the single arm data. This corresponds, however, to an impurity in the π^+ beam of only 5.10^{-4}. For the K^- beam the corresponding impurity was at a much lower level, and was due to failures in the electronics by which pions could satisfy the kaon logic. These events were also easily eliminated by cuts on the pulse heights in the beam Cerenkov counters.

For the 10.1 GeV/c single arm data on the reaction $K^-p \to \pi^-$(Missing mass) a large contribution to the trigger rate came from decays of incident kaons. $K\pi_2$ decays, when interpreted as Kp scattering, yield a missing mass above 1.5 GeV/c^2, but $K\mu_2$ decays at small angles overlap kinematically with the hypercharge exchange reactions. In order to eliminate these decays the T_5 scintillation counter array, placed behind 1.8 m of iron, was used in anticoincidence. Without any such veto the signal to noise ratio in this range of scattering angles would have been 1/40.

For the same reaction (10.1 GeV/c single arm negative) there were a considerable number of events in the mass region 0.95 - 1.30 GeV/c^2 with very small scattering angles. These events were due to an incident kaon producing a δ-ray in the target, thus giving a signal in C_1, and then another δ-ray in the T_2 scintillation counter array or in the C_2 window or gas, or decaying near the end of C_2. The measured energy of the kaon was reduced by the production of the first δ-ray and thus the calculated missing mass was larger than the proton mass. These events were only found with very small scattering angles (most below the 4 mrad cut-off imposed on the data). The contamination in the first t bin of the Σ data was only 4%.

In the 7.0 GeV/c single-arm data most of the background trigger rate was substantially reduced, since the non-interacting beam did not traverse the active areas of the spectrometer.

In the 2-arm data, backgrounds due to decays were negligible due to the further demand of a particle lying within certain limits of the calculated recoil direction. For the K-p elastic calibration data, for example, we used a cut of three times the measured standard deviation on angular precision. For the Σ production, we used a cut limit which allowed for the cone angle in the $\Sigma^+ \to p\pi^0$ decay mode.

3.3 BACKGROUNDS IN THE ANALYSED DATA

For the single arm data, the vertex position was poorly determined at small scattering angles. It was therefore necessary to eliminate non-target scattering in some way. The only significant background came from interactions in the scintillation counters immediately in front of the target. Fits made to the distribution of the reconstructed vertex along the beam direction as a function of t gave a t-independent background level of 7.5%, and thus implied a simple normalization correction. This overall level was confirmed by data taken with empty target runs and by calculation based on the amount of material in the counters.

For the 2-arm data we were able to cut safely on the vertex position because of the higher precision with which it could be determined.

3.3.1 Backgrounds specific to $\Sigma(1190)$ production

Events which satisfied all cuts yielded missing mass distributions as shown in fig. 8. Those events within the missing mass region 1.09-1.29 GeV/c^2 were taken to be Σ events. Gaussian

fits to these distributions yielded the small correction factors for the loss of events outside this mass range. The only significant background within this mass range was (in the case of the single arm data) the tail of the $\Sigma(1385)$ distribution. This background was corrected on the basis of the fits to the $\Sigma(1385)$ distributions discussed in the next section.

For the 2-arm data, the use of a very high beam intensity resulted in a small accidental contribution. Thus we have small backgrounds under the $\Sigma(1190)$ peak due to such reactions as $\pi^+p \to \pi^+\Delta^+$ and $K^-p \to K^-\Delta^+$. These backgrounds can be evaluated on the basis of the proton peak background observed in these missing mass distributions. On this basis, we estimate this background to be at worst 2% (at low $|t|$) and entirely negligible over most of the t range.

3.3.2 Backgrounds specific to $\Sigma(1385)$ production

$\Sigma^+(1385)$ cross-sections have been evaluated only from the single-arm data at each momentum. The analysis is complicated by the fact that the $\Sigma^+(1385)$ cross-sections are much smaller than those for the Σ production thereby increasing the relative effect of small backgrounds. In addition more background is anticipated in the $\Sigma(1385)$ mass range as the thresholds for various reactions open up. The procedure used in the analysis was to evaluate the cross-sections using two hypotheses for the assumed background: Fit A with zero background and Fit B with large background. This procedure has already been described in detail for the 10.1 GeV/c results [4] and examples of the fits are given in that paper. We have used the same procedure for the cross-sections at 7.0 GeV/c.

We have in addition extended our study of the backgrounds in two ways. First we have made a detailed assessment of the expected backgrounds from all relevant reactions, using measured cross-sections. This leads to a calculated background of 13%, in good agreement with the with-background fits (fits B). Secondly we have made fits which introduce the maximal background consistent with the data. These fits (called fits C) give backgrounds for both reactions of 25%. While these fits seem implausible in view of the discrepancy with the calculated background, they do serve as a caution that our $\Sigma(1385)$ cross-sections evaluated on the basis of fits A and B could be high. In the most unlikely event that one reaction could be represented by the background-free fit A, while the other reaction was correctly represented by the maximal-background fit C, the ratio of the cross-sections for the two reactions would be affected by ±25%. The errors assigned to the points on the differential cross-sections were the statistical errors to which were added in quadrature the error corresponding to the difference between fit A and fit B for that particular t bin. Fits C are considered to be sufficiently improbable that they are not allowed for in evaluating the cross-section uncertainty, except that the normalization error is increased to accommodate the results from fits C.

3.4 ACCEPTANCE CALCULATION

The acceptance of the apparatus was evaluated using a standard Monte Carlo procedure, with beam tracks from the experiment as input for the event generation. Absorption and decay corrections for the final-state particles were included. An excellent cross-check applied to the 10.1 GeV/c single-arm data was to calculate the survival probability for beam particles (particularly K^+ and π^-) and to compare this with the experimental survival probability based on finding a clean track through the forward spectrometer. Including the track reconstruction efficiency (determined from the measured spark chamber efficiencies) we found agreement between the calculated and measured survival probabilities of better than 1%.

To test further the accuracy and stability of the acceptance calculation we artificially decreased the geometrical aperture by imposing geometrical cuts on the data and the Monte Carlo generated events. In fig. 9 is shown the number of events, for the low intensity $\pi^+p \rightarrow K^+\Sigma^+$ data, corrected for acceptance in each t' bin for five different acceptance cuts. The figure also shows the corresponding acceptance curves. As can be seen the variations in the number of events corrected for the geometrical acceptance are very small although the acceptance is decreased in some bins by a factor four.

For the 2-arm data it was furthermore necessary to calculate the acceptance of the recoil particle in the side arm detectors. In addition to the geometrical aperture, cuts were imposed on the recoil particle which corresponded exactly to those used on the real data, namely a t-dependent cone based on the precision in determining the recoil direction for elastic scattering, and the same thing expanded further by the $\Sigma \rightarrow p\pi^0$ decay cone angle for Σ reactions.

3.5 NORMALIZATION PROCEDURES

3.5.1 Geometry 1

For the Σ production reactions, the normalization procedure has already been been described in some detail [3 and 5]. In evaluating the differential cross-sections, it was necessary to know

1. the efficiency with which incident π^+ or K^- would survive the cuts on beam Cerenkov pulse heights, beam track reconstruction via the hodoscopes, etc. Such effects were evaluated using a sample of incident beam triggers which was taken in parallel with the hypercharge exchange triggers.

2. the contamination from other particle types (e.g. e^+ and μ^+) in the incident beam signals (e.g. π^+). These small effects were measured in an independent experiment.

3. the efficiency with which forward scattered K^+ or π^- would survive the cuts on C_1 and C_2 pulse heights, reconstruction of the particle trajectory in the forward spectrometer, etc. Such effects could again be evaluated

in a purely empirical manner using samples of triggers of incident K^+ and π^- which were also taken in parallel with the hypercharge exchange triggers. Subjecting these events to the standard cuts, we evaluated the efficiencies which were used in calculating the cross-sections. In fact these acceptances agree well with independent calculations based on individual spark chamber efficiencies (typically 99.1%), amount of material in the spectrometer, etc.

As an empirical check of the sensitivity to random background tracks we ran half of the positive data at 3 times the normal intensity. The differential cross-section for these data agrees very well in normalization with the normal intensity data, and in particular shows no discrepancy in the first t bin.

3.5.2 Geometry 2

The normalization factors used for the incident beam and the forward arm were obtained in the same way as for geometry 1, with additional factors due to the larger angular range which implied small corrections for the varying amount of material transversed.

For the recoil arm the procedure used was less direct, being more similar to that conventionally used for acceptance calculations. In order to test this procedure, a substantial quantity of K^-p elastic scattering data was taken at 10.1 GeV/c, mixed in with the hypercharge exchange triggers. The normalization procedure was as follows.

1. We used a Monte Carlo acceptance program to evaluate the side-arm acceptance, including the geometrical apertures of the spark chambers and T_3 array, as well as the effects of secondary interactions, multiple scattering and range. This calculation was particularly well tested by the small $|t|$ elastic data, for which the corrections were very large. Having obtained correct results in this case, one could be fully confident about the hypercharge exchange reactions, where the smearing effects of the Σ decay made for much smaller corrections at all t values.

2. Due to the problem of hadron showers from upstream interactions sometimes confusing the pattern recognition in the side arm (mentioned in 3.1) it was necessary to evaluate the reconstruction efficiency for the spark chambers in a way which took account of the correlated loss of information from several planes together. The elastic triggers were ideal for this purpose, since the reconstruction of the forward track, plus a missing mass cut, gave a clean sample of elastic events for which the recoil direction could be determined. For those events where this lay within the spark chamber aperture, one could ask whether the side arm track reconstruction program found the appropriate track. In this way the side arm track reconstruction efficiency was found to be 88±1%, independent of the track position within the chambers. For the hypercharge exchange events, this procedure could not be followed due to the lack of knowledge of the direction of the Σ decay products, but

the reconstruction efficiency determined from the elastic triggers taken at the same time, could obviously be used with complete confidence.

As a check on the overall procedure, we compared our differential cross-sections for the K^-p elastic scattering with the data of Bartsch et al. [10]. The ratio of our cross-sections with respect to these published data is 0.988±0.025, with no evidence for any t dependence. (The error quoted is purely statistical and excludes the systematic normalization uncertainty, estimated to be 2% in the data of Bartsch et al. and 5% in our data).

For the hypercharge exchange reactions we were able to compare the cross-sections from the 1-arm and 2-arm triggers, since at both momenta we had a substantial overlap in the t range covered (-0.05 to -0.30 $(GeV/c)^2$). Using the appropriate acceptance factors and spark chamber efficiencies, the 1-arm and 2-arm cross-sections over this t range were found to agree in all cases to better than 10%, and in particular for the high statistics 10.1 GeV/c data on the reaction $\pi^+p \rightarrow K^+\Sigma^+$, to agree to 1±6%. As already discussed in [5] our final procedure was to normalize the 2-arm results to match the more precise 1-arm data in the overlap region of t.

The consistency checks on the elastic data and hypercharge exchange data lead to a final normalization precision of 5% for the Σ production reactions.

3.5.3 Σ(1385) reactions

For the Σ(1385) production reactions, the basic procedure was identical, with the complication that we have an additional uncertainty due to the various possible backgrounds already discussed. These factors lead to a normalization precision on the Σ(1385) cross-sections of +10% -30%.

3.6 POLARIZATION CALCULATION

In the 2-arm data, the Σ polarization as a function of t was evaluated by measuring the asymmetry (U-D)/(U+D) where U and D are respectively the number of events where the observed recoil particle is above or below the scattering plane as defined by the measured incident beam and forward particle directions.

The following factors were taken into account:-

1. possible systematic errors due to geometrical errors between the 3 arms of the detection system (these were aligned accurately using coplanar elastic scattering data)

2. smearing due to the measurement precision (especially at low $|t|$)

3. dilution of the asymmetry by the small contamination from $\Sigma^+ \rightarrow n\pi^+$ decays within the $\Sigma^+ \rightarrow p\pi^0$ decay cone

These effects were included in the Monte Carlo calculation, which was then used to determine the relationship between the experimental asymmetry and the polarization.

4. RESULTS AND DISCUSSION

4.1 Σ PRODUCTION REACTIONS

The differential cross-sections and polarizations are plotted in figs. 10 and 11, and are listed in tables 2 and 3. Parameters of the exponential fits to the small $|t|$ region (< 0.4 (GeV/c)^2) are given in table 4.

Comparisons have been made with existing data for these processes. At 7.0 GeV/c our cross-sections for reaction (1) agree well with those of Pruss et al. [11] and Baker et al. [12] as shown in fig. 12. At 10.1 GeV/c we have compared with Bashian et al. [13] and Ballam et al. [14]. In the latter case the cross-sections have been scaled to allow for the momentum difference between the experiments (11.5 and 10.1 GeV/c). There is good general agreement (fig. 13) except at large $|t|$ values. In figs. 14 and 15 we plot the differential cross-sections for reaction (2) at 7.0 and 10.1 GeV/c respectively and compare them with the results of Baker et al. [12] at 7.0 GeV/c and Ballam et al. [14] at 11.5 GeV/c (again scaled to 10.1 GeV/c). The agreement is excellent.

In fig. 16 the s-dependence of the differential cross-sections at t=0 for both reactions is shown for a selection of experiments. These reveal a smooth s-dependence of converging cross-sections with the intriguing suggestion that they may cross over as s increases above about 20 (GeV)^2.

By using results from several experiments (details have already been given in an earlier paper [5]), we have determined values of $\alpha_{eff}(t)$. These are plotted in fig. 17.

4.1.1 Features of the results

The important features to note are the near equality of the cross-sections for $|t'| < 0.2$ (GeV/c)^2 at 10.1 GeV/c, whereas at 7.0 GeV/c they are significantly different in the same t range. This is illustrated in fig. 18 which shows the relative cross-section differences Δ (plotted against t') where

$$\Delta = \frac{d\sigma/dt'(K^-p\to\pi^-\Sigma^+) - d\sigma/dt'(\pi^+p\to K^+\Sigma^+)}{d\sigma/dt'(K^-p\to\pi^-\Sigma^+) + d\sigma/dt'(\pi^+p\to K^+\Sigma^+)}$$

At 7.0 GeV/c the values of Δ are approximately twice as large as those at 10.1 GeV/c in the region $|t'| < 0.5$ (GeV/c)^2. This behaviour of the cross-section differences has been confirmed in another experiment where both reactions have been measured at 7.0 [12] and 11.5 GeV/c [14].

Between t' = -0.5 and t' = -1.0 (GeV/c)² at both momenta, the cross-sections cross over (where α_{eff} values lie close to the K*-K** trajectory).

For |t'| > 1.0 (GeV/c)² the cross-sections are flatter and appear not to be converging as the momentum is increased from 7.0 to 10.1 GeV/c.

The polarizations achieve large absolute values and exhibit approximate mirror symmetry at both incident momenta. This feature has also been confirmed by the experiment at 7.0 and 11.5 GeV/c [15].

Thus at 10.1 GeV/c there is only a small discrepancy with the predictions of weak exchange degeneracy in the small |t| region, whereas at 7.0 GeV/c the results are inconsistent with this prediction. Strong exchange degeneracy is not satisfied at either momentum.

Finally a test can be made for the presence of an I=3/2 exchange amplitude in the t-channel. A pure I=1/2 exchange predicts that

$$d\sigma/dt(\pi^+p\to K^+\Sigma^+) = 2\, d\sigma/dt(\pi^-p\to K^0\Sigma^0)$$

This comparison in made in fig. 19, where our results at 7.0 GeV/c have been scaled to 6.0 GeV/c and plotted with the results of Ward et al. [19]. The agreement is striking and confirms the dominance of the I=1/2 exchange. Similarly at 10.1 GeV/c comparing with the data of Foley et al. [20], we have found excellent agreement throughout the t range.

4.2 Σ(1385) PRODUCTION REACTIONS

The differential cross-sections for the Σ(1385) reactions are shown in figs. 20 and 21 and are listed in table 5. The number of events were taken from the mass fits described in 3.3.2, using the averages of the two values obtained from fits A and B.

4.2.1 Features of the results

At both incident momenta the differential cross-sections plotted against t' show no significant differences of shape, in contrast to the Σ production reactions. The measured difference between the cross-sections is subject to the uncertainty in normalization on each reaction. Taking the full range allowed by the data (Fits A as one extreme and Fits C as the other) we obtain relative cross-section differences Δ (defined as for the Σ production, but now integrated through the t' range of our experiment), of

0.36 ± 0.15 (systematic) ± 0.04 (statistical) at 7.0 GeV/c
(t'=0 to -0.5 (GeV/c)²)

0.33 ± 0.15 (systematic) ± 0.04 (statistical) at 10.1 GeV/c
(t'=0 to -0.3 (GeV/c)²)

It should be noted that the systematic errors given are not standard deviations but extreme limits resulting from rather

implausible combinations of zero background for one reaction and maximal background for the other. We can conclude that these reactions, which appear to be spin-flip dominated, do not satisfy the prediction of equal cross-sections at either momentum.

4.2.2 Comparison with other experiments

In fig. 22 we have plotted all the integrated cross-sections for $\Sigma(1385)$ production in reactions (3) and (4) above 3 GeV/c, for the range of t' 0 to -1.0 $(GeV/c)^2$, using an exponential extrapolation in cases where a smaller t' range was covered in the experiment. For both reactions, there are inconsistencies by factors of 2 between various experiments whatever s dependence one assumes, and these inconsistencies are not resolved by rejecting any one experiment from the plot.

Therefore, in order to assess the exchange degeneracy situation, it seems safest to take pairs of reactions from one experiment, where the systematic effects are generally similar and will tend to cancel. Apart from our experiment there is only one other [22] which has measured both reactions. As can be seen from fig. 22, although we differ in absolute normalization, the results from the pairs of reactions at 7.0, 7.0, 10.1 and 11.5 GeV/c all agree in finding substantial cross-section differences, which are (within the errors) independent of s. This is in conflict with the naive expectations of exchange degeneracy. Cautis et al. [27] have explained some (about half) of the cross-section differences at 11.5 GeV/c as being due to t_{min} effects. The remaining differences lie within the systematic errors of their experiment so they conclude that the data are consistent with the exchange degeneracy hypothesis. Due to the large errors on the measured cross-sections, this conclusion remains rather weak, and of course the assessment of the t_{min} effects is model dependent. Thus we prefer to avoid drawing any definitive conclusions about the status of exchange degeneracy with respect to our measured $\Sigma(1385)$ cross-sections, but rather to allow the models to confront the large cross-section differences present in the data.

4.3 THEORETICAL INTERPRETATIONS

No existing phenomenology describes quantitatively the scattering data for two body elastic and inelastic reactions. Early efforts to understand hypercharge exchange results achieved only limited success because of

1. the absence of a complete set of accurate measurements (e.g. $d\sigma/dt$, P, A, R etc), which meant that theoretical models had to be used and

2. the inherently mixed nature of K* and K** exchange.

For example, Irving et al. [28], attempted to gain insight into the polarization and line reversal breaking observed in hypercharge exchange reactions by assuming exchange degenerate poles where

1. the spin flip terms were not absorbed and

2. the non flip terms were absorbed with the Pomeron

Fits were made to the $KN \to \pi Y$ data and then predictions were made for the corresponding $\pi N \to KY$ results. The polarization predictions were good but the $K^- p \to \pi^- \Sigma^+$ reaction was more absorbed than the $\pi^+ p \to K^+ \Sigma^+$ one, which consequently had a larger cross-section, in contradiction with the experimental data.

An alternative approach by Irving et al. [29] theoretically constrained the spin flip term to be pure EXD and then solved algebraically for the non flip amplitudes using experimental results at 4 and 14 GeV/c. However a subsequent analysis of KN charge exchange scattering (spin flip dominated) has revealed some exchange degeneracy breaking for the ρ and A_2 trajectories ($\alpha_\rho - \alpha_{A_2} = 0.1$) [30]. Irving and Worden [31] then assumed a similar breaking for the K* and K** trajectories and repeated the analysis. However, this work was not conclusive due to

1. prejudice about how the spin flip term behaves

2. ambiguities in the solutions and

3. the uncertainties introduced by the experimental data (accurate line reversal comparisons were specifically requested in the conclusions).

Several alternative attempts to understand the line reversal breaking in hypercharge exchange processes have been made: for example

1. Auvil et al. [32] used a simple model containing broken exchange degeneracy of the leading trajectories (in this case K* and K**) and requiring secondary (low lying) trajectories in order to describe both the cross-section differences and their t-dependence. However, this predicts that the difference decreases only slowly as the energy increases.

2. Similarly the complex Regge pole model of Roy et al. [33] predicted that large cross-section differences persist at high energies.

3. An empirical approach by Ringland et al. [34] proposed a conventional pole plus absorption model, but introduced an arbitrary phase modification (a rotation of $\pi/2$) into the absorptive cut for the exotic process ($Kp \to \pi\Sigma$). There is no compelling theoretical justification for such a model.

More recently, Navelet and Stevens [35] have performed an amplitude parametrisation based on a Regge pole plus effective cut model in an effort to establish the systematics for K* and K** exchange above 3 GeV/c. Here again the assumption was made that the spin flip amplitude had no cuts. The trajectories and residues were allowed to be non exchange degenerate. The fit, which was made before the present results and those of the SLAC/IC group [12,14], allowed all the experimental normalizations to vary within the quoted errors. Results from the fit are given in fig. 23, at 7.0 and 10.1 GeV/c together with our results, and clearly fail to reproduce the approach to line reversal invariance as established (for $|t| < 0.2$ (GeV/c)^2) by the recent accurate measurements, and also supported by the results at 14 and 16 GeV/c [13, 17, and 18].

A more promising approach appears to be that of Girardi [36], who used a dual Regge cut model for hypercharge exchange scattering, based on an earlier model which had been applied to πN and KN scattering [37]. This model relates the K* and K** couplings to the ρ and A_2 coupling using SU(2) and SU(3) relations. The hypercharge exchange amplitudes are essentially predicted using the ρ and A_2 amplitudes previously determined [37], with the only free parameters being the K*-K** trajectory function $\alpha(t)$ ($\alpha(t)=0.37+0.79t$) and a mass scale. An important feature of the model is the introduction of Regge-Regge cuts with absorptive corrections (via the Pomeron).

In particular the Regge-Pomeron-Regge term is claimed to be responsible for the line reversal breaking seen at lower momenta (predicting a breaking of the correct sign). It is predicted that at 10 GeV/c and above the effect of this term should be small and that the cross-sections should approach equality, in agreement with the results.

5. CONCLUSIONS

For the Σ production processes, the large polarization values attained in both reactions by $|t| \simeq 0.5$ (GeV/c)^2 rule out strong exchange degeneracy. The weak exchange degeneracy predictions of polarizations equal in magnitude but of opposite sign is well satisfied. However, the prediction of equal cross-sections is not satisfied at all for the lower momentum and only satisfied in the small $|t|$ region for the higher momentum (10.1 GeV/c). The data at large $|t|$ show the largest deviations, with no clear improvement by 10.1 GeV/c. The presence of a cross-over in the cross-sections which occurs at a rather constant t (probably all the way from 4 to 12 GeV/c) is suggestive of some consistent pattern in the exchange degeneracy breaking. The general trend is clearly for the weak exchange degeneracy predictions to improve with s; it will be extremely interesting to see measurements of both reactions in one setup in the 100 GeV energy range.

The situation with respect to the $\Sigma(1385)$ production processes is less clear. Both experiments which have measured both the K^- and π^+ reactions in a single setup find the K^- reaction to have a significantly larger cross-section with no clear signs of convergence as the energy increases, in conflict with the simple predictions of exchange degeneracy. On the other hand, the theoretical interpretation may be confused by t_{min} effects. It will be very interesting to have precise measurements at yet higher energies, where the kinematic effects should be negligible, to see if the cross-section differences remain.

6. ACKNOWLEDGEMENTS

We are very grateful for the services provided by the Science Research Council at the Rutherford Laboratory, in particular, the excellent support we have received from the Physics Apparatus Group. We also thank Mrs G. Blakely for her assistance in some of the data processing and checking. All of the efforts of the EP Division at CERN in bringing this experiment to a satisfactory conclusion are sincerely appreciated. We must also thank P. Anzoli, R. Audria, M. Burns, P. Helgaker, D.L. Hill, R. Kiesler, J. Lindsay, B. Mouellic, H.I. Pizer, D. Ploujoux and O. Sorum for their help throughout the experiment.

REFERENCES

[1] K. W. Lale and J Louie, Nucl. Phys. B19(1970)205; J Mandula et al., Ann. Rev. Nucl. Sci. 20(1970)289.

[2] V D Barger and D B Cline, Phenomenological theories of high energy scattering (W A Benjamin, New York, 1969)

[3] A Berglund et al., Phys. Letters 57B(1975)100.

[4] A Berglund et al., ibid 60B(1975)117.

[5] A Berglund et al., ibid 73B(1978)369.

[6] A Berglund et al., Nucl. Phys. B 137(1978)276.

[7] H Hinterberger and R Winston, Rev. Sci. Instr. 37(1966)1094.

[8] H I Pizer, Nucl. Instr. and Methods 93(1971)249.

[9] A Berglund et al. (following paper)

[10] J Bartsch et al., Nucl. Phys. B 29(1971)398.

[11] S M Pruss et al., Phys. Rev. Letters 23(1969)189.

[12] P A Baker et al., (private communication).

[13] A Bashian et al., Phys. Rev. D4(1971)2667.

[14] J Ballam et al., Phys. Rev. Letters 41(1978)676.

[15] P A Baker et al., Phys. Rev. Letters 40(1978)678.

[16] G G G Massaro et al., Phys. Letters 66B(1977)385.

[17] B Chaurand et al., Nucl. Phys. B 117(1976)1.

[18] D Birnbaum et al., Phys. Letters 31B(1970)484.

[19] C E Ward et al., Phys. Rev. Letters 31(1973)1149.

[20] K J Foley et al., Phys. Rev. D8(1973)27.

[21] S O Holmgren et al., Nucl. Phys. B119(1977)261.

[22] P A Baker et al., SLAC-PUB 2169(1978).

[23] E Bracci et al., High Energy Reactions Analysis Group, CERN/HERA 72-1(1972); ibid 72-2(1972).

[24] M Aguilar-Benitez et al., Phys. Rev. D 6(1972)29.

[25] D Z Toet et al., Nucl. Phys. B63(1973)248.

[26] M C Goddard et al., BNL-23740.

[27] C V Cautis et al., SLAC-PUB 2233(1978).

[28] A C Irving et al., Nucl. Phys. B32(1971)1.

[29] A C Irving et al., Nuovo Cimento 16A(1973)573.

[30] F Elvekjaer and R C Johnson,
Nucl. Phys. B83(1974)142.

[31] A C Irving and R P Worden,
Physics Reports 34(1977)117.

[32] P R Auvil et al., Phys. Letters 31B(1970)303.

[33] D P Roy et al., Phys. Letters 34B(1971)512.

[34] G A Ringland et al., Nucl. Phys. B44(1972)395.

[35] H Navelet and P R Stevens, Nucl. Phys. B104(1976)171

[36] G Girardi, J Phys. G 3(1977)1031.

[37] G Girardi et al., Nucl. Phys. B 69(1974)107.

TABLE 1. Beam composition as a fraction of momentum and polarity.

Momentum (GeV/c)	Polarity	Beam fractions (%) $\pi+\mu+e$	K	p
10.1	+	15.9	1.1	83.0
10.1	-	98.5	1.1	0.4
7.0	+	40.5	2.4	56.9
7.0	-	97.7	1.3	1.0

TABLE 2. Differential cross-sections for the Σ production reactions. Errors listed are statistical. In addition we estimate a maximum systematic normalization error of 5%.

Reaction $\pi^+p \to K^+\Sigma^+$ at 7.0 GeV/c momentum

t' $(GeV/c)^2$	t $(GeV/c)^2$	bin width $(GeV/c)^2$	$d\sigma/dt$ $\mu b/(GeV/c)^2$	error $\mu b/(GeV/c)^2$
-0.055	-0.0650	0.01	160.0	28.2
-0.070	-0.0800	0.02	172.5	15.9
-0.090	-0.1000	0.02	119.0	10.3
-0.110	-0.1200	0.02	124.4	7.8
-0.140	-0.1500	0.04	93.4	5.0
-0.180	-0.1900	0.04	65.0	3.8
-0.220	-0.2300	0.04	42.2	2.9
-0.260	-0.2700	0.04	27.0	2.3
-0.310	-0.3200	0.06	21.1	1.7
-0.370	-0.3800	0.06	11.3	1.2
-0.500	-0.5100	0.20	6.21	0.50
-0.700	-0.7100	0.20	4.10	0.47
-0.900	-0.9100	0.20	3.80	0.46
-1.100	-1.1100	0.20	3.45	0.45
-1.300	-1.3100	0.20	2.06	0.36
-1.500	-1.5100	0.20	1.66	0.32
-1.700	-1.7100	0.20	0.71	0.22
-1.900	-1.9100	0.20	0.35	0.18

Reaction $K^-p \to \pi^-\Sigma^+$ at 7.0 GeV/c momentum

t' $(GeV/c)^2$	t $(GeV/c)^2$	bin width $(GeV/c)^2$	$d\sigma/dt$ $\mu b/(GeV/c)^2$	error $\mu b/(GeV/c)^2$
-0.055	-0.0463	0.01	353.8	41.3
-0.070	-0.0613	0.02	284.6	16.0
-0.090	-0.0813	0.02	255.3	11.2
-0.110	-0.1013	0.02	235.7	11.1
-0.140	-0.1313	0.04	171.3	7.5
-0.180	-0.1713	0.04	132.4	6.4
-0.220	-0.2113	0.04	100.7	5.6
-0.260	-0.2513	0.04	78.6	5.0
-0.310	-0.3013	0.06	49.6	3.3
-0.370	-0.3613	0.06	33.9	2.8
-0.500	-0.4913	0.20	15.7	1.1
-0.700	-0.6913	0.20	6.78	1.24
-0.900	-0.8913	0.20	3.52	0.92
-1.100	-1.0913	0.20	3.14	0.88
-1.300	-1.2913	0.20	1.06	0.53
-1.500	-1.4913	0.20	0.87	0.51
-1.700	-1.6913	0.20	0.62	0.44

TABLE 2 (continued).

Reaction $\pi^+p \to K^+\Sigma^+$ at 10.1 GeV/c momentum

t' $(GeV/c)^2$	t $(GeV/c)^2$	bin width $(GeV/c)^2$	$d\sigma/dt$ $\mu b/(GeV/c)^2$	error $\mu b/(GeV/c)^2$
-0.005	-0.0117	0.01	243.3	9.4
-0.015	-0.0217	0.01	230.8	8.2
-0.025	-0.0317	0.01	200.9	7.5
-0.035	-0.0417	0.01	183.2	7.3
-0.045	-0.0517	0.01	174.2	7.4
-0.055	-0.0617	0.01	142.2	7.2
-0.065	-0.0717	0.01	146.8	8.1
-0.080	-0.0867	0.02	118.0	5.7
-0.100	-0.1067	0.02	103.4	6.1
-0.130	-0.1367	0.04	78.1	4.8
-0.175	-0.1817	0.05	53.3	4.2
-0.225	-0.2317	0.05	29.4	1.7
-0.275	-0.2817	0.05	18.5	1.0
-0.325	-0.3317	0.05	12.6	0.9
-0.375	-0.3817	0.05	9.25	0.71
-0.425	-0.4317	0.05	5.87	0.55
-0.475	-0.4817	0.05	4.25	0.46
-0.550	-0.5567	0.10	3.64	0.31
-0.650	-0.6567	0.10	2.79	0.27
-0.750	-0.7567	0.10	2.43	0.25
-0.875	-0.8817	0.15	1.90	0.18
-1.025	-1.0317	0.15	1.45	0.16
-1.200	-1.2067	0.20	1.16	0.13
-1.400	-1.4067	0.20	0.85	0.11
-1.625	-1.6317	0.25	0.47	0.07
-1.875	-1.8817	0.25	0.22	0.05
-2.125	-2.1317	0.25	0.20	0.05
-2.500	-2.5067	0.50	0.04	0.02

Reaction $K^-p \to \pi^-\Sigma^+$ at 10.1 GeV/c momentum

t' $(GeV/c)^2$	t $(GeV/c)^2$	bin width $(GeV/c)^2$	$d\sigma/dt$ $\mu b/(GeV/c)^2$	error $\mu b/(GeV/c)^2$
-0.005	0.0011	0.01	301.0	27.4
-0.015	-0.0089	0.01	278.7	19.6
-0.025	-0.0189	0.01	222.2	16.9
-0.035	-0.0289	0.01	222.9	17.2
-0.045	-0.0389	0.01	225.5	18.1
-0.055	-0.0489	0.01	194.7	18.0
-0.065	-0.0589	0.01	171.2	18.4
-0.080	-0.0739	0.02	170.0	14.8
-0.100	-0.0939	0.02	158.0	16.7
-0.130	-0.1239	0.04	111.7	12.4
-0.175	-0.1689	0.05	74.3	6.8
-0.225	-0.2189	0.05	43.4	4.8
-0.275	-0.2689	0.05	28.1	3.9
-0.350	-0.3439	0.10	18.9	2.6
-0.500	-0.4939	0.20	7.97	1.20
-0.750	-0.7439	0.30	2.16	0.50
-1.100	-1.0939	0.40	0.60	0.23
-1.650	-1.6439	0.70	0.28	0.13

TABLE 3. Polarizations for the Σ production reactions. The errors are statistical.

Reaction $\pi^+p \to K^+\Sigma^+$ at 7.0 GeV/c momentum

t $(GeV/c)^2$	bin width $(GeV/c)^2$	polarization	error
-0.060	0.04	-0.03	0.26
-0.110	0.06	-0.14	0.13
-0.170	0.06	0.11	0.15
-0.300	0.20	0.23	0.12
-0.500	0.20	0.54	0.23
-0.800	0.40	0.72	0.21
-1.200	0.40	0.49	0.25
-1.700	0.60	0.09	0.36

Reaction $K^-p \to \pi^-\Sigma^+$ at 7.0 GeV/c momentum

t $(GeV/c)^2$	bin width $(GeV/c)^2$	polarization	error
-0.080	0.08	-0.37	0.21
-0.160	0.08	-0.12	0.23
-0.300	0.20	-0.22	0.19
-0.600	0.40	-0.47	0.27
-1.200	0.80	-0.51	0.41

Reaction $\pi^+p \to K^+\Sigma^+$ at 10.1 GeV/c momentum

t $(GeV/c)^2$	bin width $(GeV/c)^2$	polarization	error
-0.185	0.03	0.16	0.29
-0.225	0.05	0.21	0.16
-0.275	0.05	0.39	0.17
-0.350	0.10	0.66	0.14
-0.500	0.20	1.12	0.14
-0.700	0.20	0.94	0.17
-0.950	0.30	0.61	0.19
-1.300	0.40	0.53	0.19
-1.750	0.50	0.16	0.31

Reaction $K^-p \to \pi^-\Sigma^+$ at 10.1 GeV/c momentum

t $(GeV/c)^2$	bin width $(GeV/c)^2$	polarization	error
-0.125	0.05	-0.22	0.28
-0.200	0.10	0.03	0.22
-0.350	0.20	-0.39	0.24
-0.675	0.45	-1.04	0.33
-1.450	1.10	0.13	0.67

TABLE 4. Parameters of exponential fits to $d\sigma/dt$. The differential cross-sections are fitted in the range $0 < |t| < 0.4$ $(GeV/c)^2$ to the form $d\sigma/dt = A\, e^{bt}$

7.0 GeV/c	$\pi^+p \to K^+\Sigma^+$	A= 338.0 ± 8.1	$\mu b/(GeV/c)^2$
		b= 8.96 ± 0.12	$(GeV/c)^{-2}$
	$K^-p \to \pi^-\Sigma^+$	A= 462.1 ± 8.2	$\mu b/(GeV/c)^2$
		b= 7.30 ± 0.08	$(GeV/c)^{-2}$
10.1 GeV/c	$\pi^+p \to K^+\Sigma^+$	A= 273.1 ± 3.4	$\mu b/(GeV/c)^2$
		b= 9.39 ± 0.09	$(GeV/c)^{-2}$
	$K^-p \to \pi^-\Sigma^+$	A= 292.4 ± 7.4	$\mu b/(GeV/c)^2$
		b= 8.36 ± 0.08	$(GeV/c)^{-2}$

TABLE 5. Differential cross-sections for the $\Sigma(1385)$ production reactions. Errors listed combine the statistical uncertainties and the background uncertainties for fits A and B for each t' bin. In addition we estimate a maximum normalization error of +10%, -30%.

Reaction $\pi^+p \to K^+\Sigma^+(1385)$ at 7.0 GeV/c momentum

t' $(GeV/c)^2$	bin width $(GeV/c)^2$	$d\sigma/dt$ $\mu b/(GeV/c)^2$	error $\mu b/(GeV/c)^2$
-0.060	0.04	44.1	8.4
-0.100	0.04	51.9	6.4
-0.140	0.04	43.8	7.0
-0.180	0.04	41.0	6.7
-0.220	0.04	36.1	6.4
-0.260	0.04	34.1	5.8
-0.310	0.06	25.8	4.8
-0.370	0.06	19.0	4.1
-0.500	0.20	10.8	2.3

Reaction $K^-p \to \pi^-\Sigma^+(1385)$ at 7.0 GeV/c momentum

t' $(GeV/c)^2$	bin width $(GeV/c)^2$	$d\sigma/dt$ $\mu b/(GeV/c)^2$	error $\mu b/(GeV/c)^2$
-0.060	0.04	94.3	8.9
-0.100	0.04	100.6	5.8
-0.140	0.04	88.6	5.8
-0.180	0.04	84.5	5.8
-0.220	0.04	77.4	6.1
-0.260	0.04	73.7	5.8
-0.310	0.06	54.0	4.3
-0.370	0.06	47.0	4.1
-0.500	0.20	26.8	2.0

Reaction $\pi^+p \to K^+\Sigma^+(1385)$ at 10.1 GeV/c momentum

t' $(GeV/c)^2$	bin width $(GeV/c)^2$	$d\sigma/dt$ $\mu b/(GeV/c)^2$	error $\mu b/(GeV/c)^2$
-0.005	0.01	7.2	5.4
-0.015	0.01	15.8	7.6
-0.030	0.02	27.4	6.5
-0.050	0.02	28.5	4.3
-0.080	0.04	29.4	4.0
-0.125	0.05	36.8	5.2
-0.175	0.05	24.8	4.5
-0.225	0.05	30.0	5.2
-0.275	0.05	22.0	4.5

Reaction $K^-p \to \pi^-\Sigma^+(1385)$ at 10.1 GeV/c momentum

t' $(GeV/c)^2$	bin width $(GeV/c)^2$	$d\sigma/dt$ $\mu b/(GeV/c)^2$	error $\mu b/(GeV/c)^2$
-0.010	0.02	20.3	9.1
-0.040	0.04	43.5	6.7
-0.080	0.04	58.4	8.2
-0.125	0.05	73.3	10.5
-0.175	0.05	57.1	11.0
-0.250	0.10	52.8	8.1

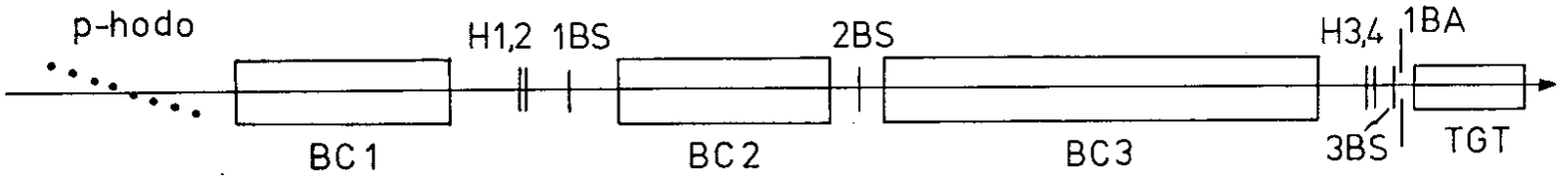

Fig. 1 Layout of the incident beam for the 10.1 GeV/c part of the experiment. BC1 to BC3 are threshold Cerenkov counters, 1BS to 3BS are scintillation counters, 1BA is a halo counter (to veto beam halo), H1 to H4 are finger scintillation counters (to measure the position and the direction of incident particle), p-hodo is the beam momentum hodoscope and TGT is the hydrogen target. The figure is not to scale.

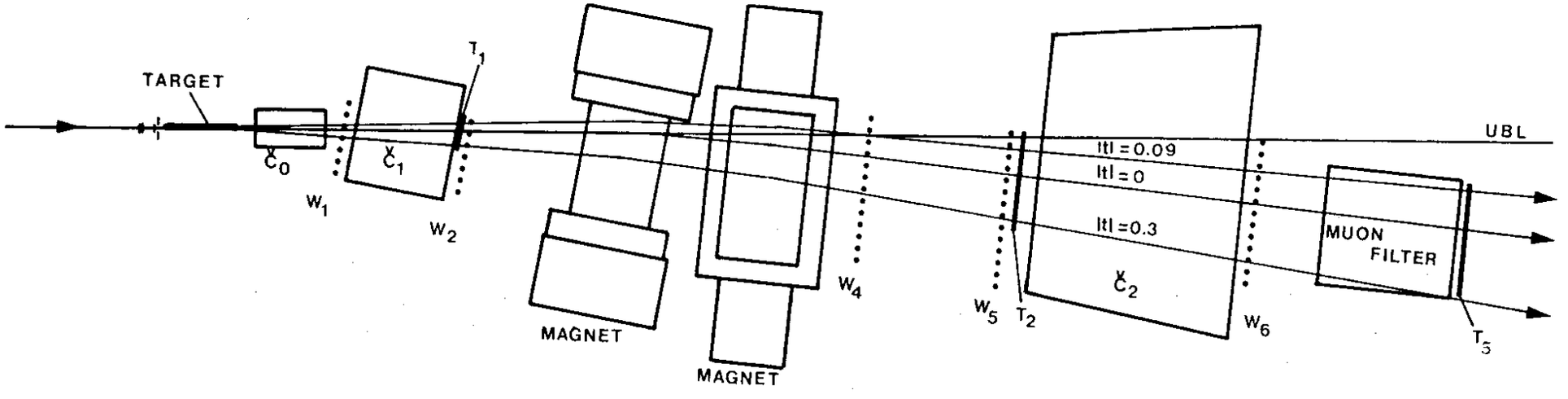

Fig. 2 Layout of the spectrometer for the small angle geometry (geometry 1). C_0, C_1, and C_2 are threshold Cerenkov counters. T_1, T_2, and T_3 are scintillation counter arrays. W_1 to W_6 are modules of spark-chambers. The muon filter consisted of 1.8 m of iron. UBL is the Undeflected Beam Line. A few particle trajectories are indicated.

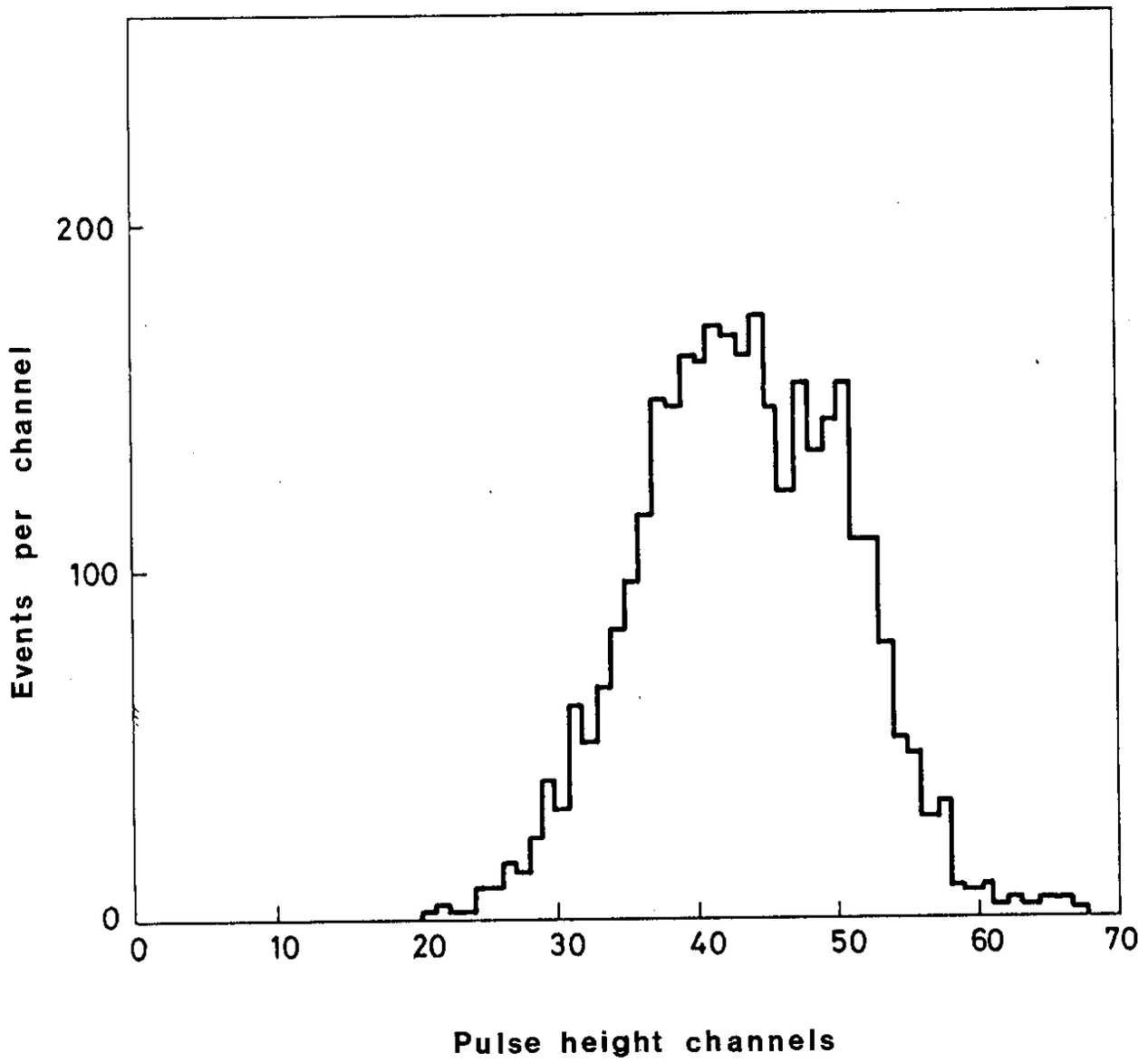

Fig. 3 A pulse height spectrum of C_1 showing the response to 10 GeV/c kaons, with protons below threshold. Phototube noise pulses were below 10 channels.

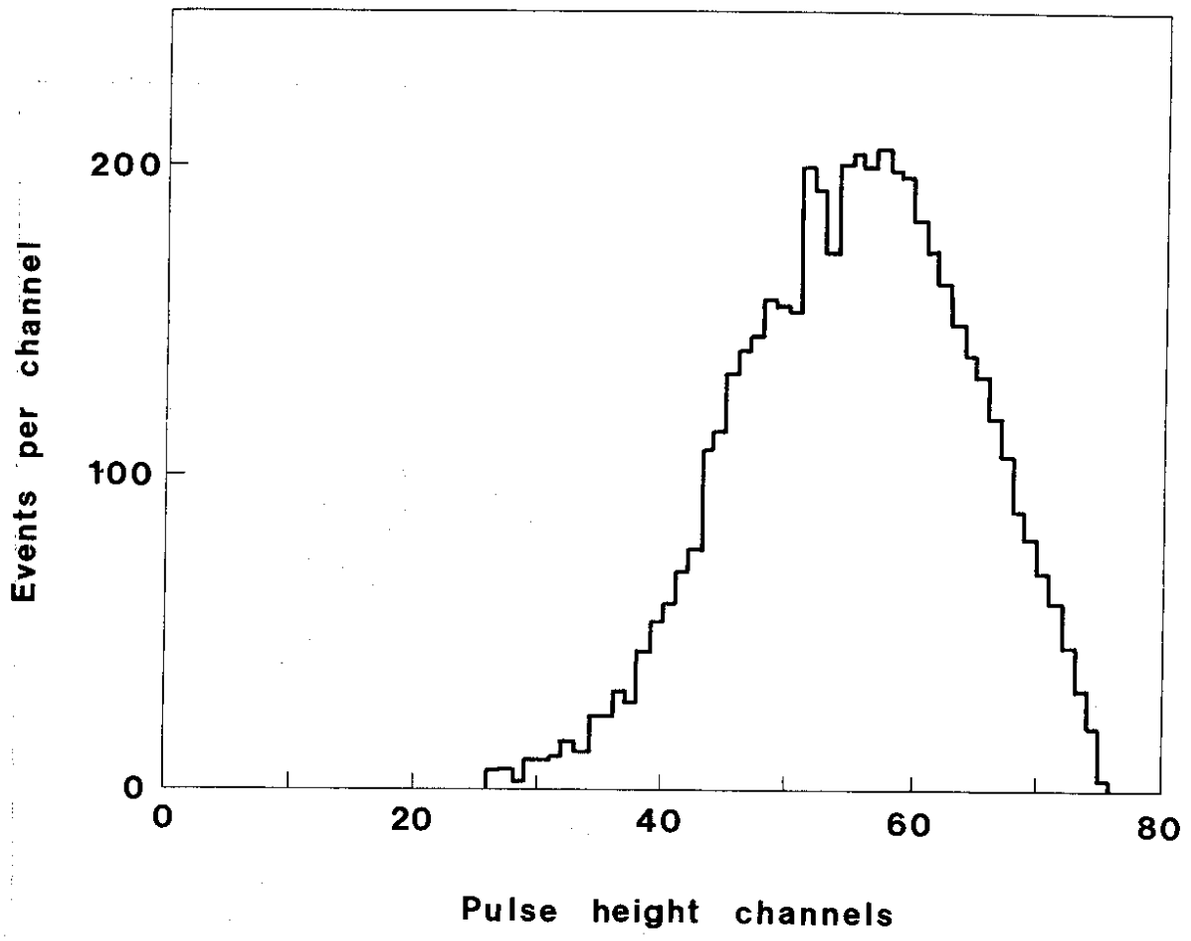

Fig. 4 A pulse height spectrum of C_2 showing the response to 10.1 GeV/c pions, with kaons and protons below threshold. Phototube noise pulses were below 15 channels.

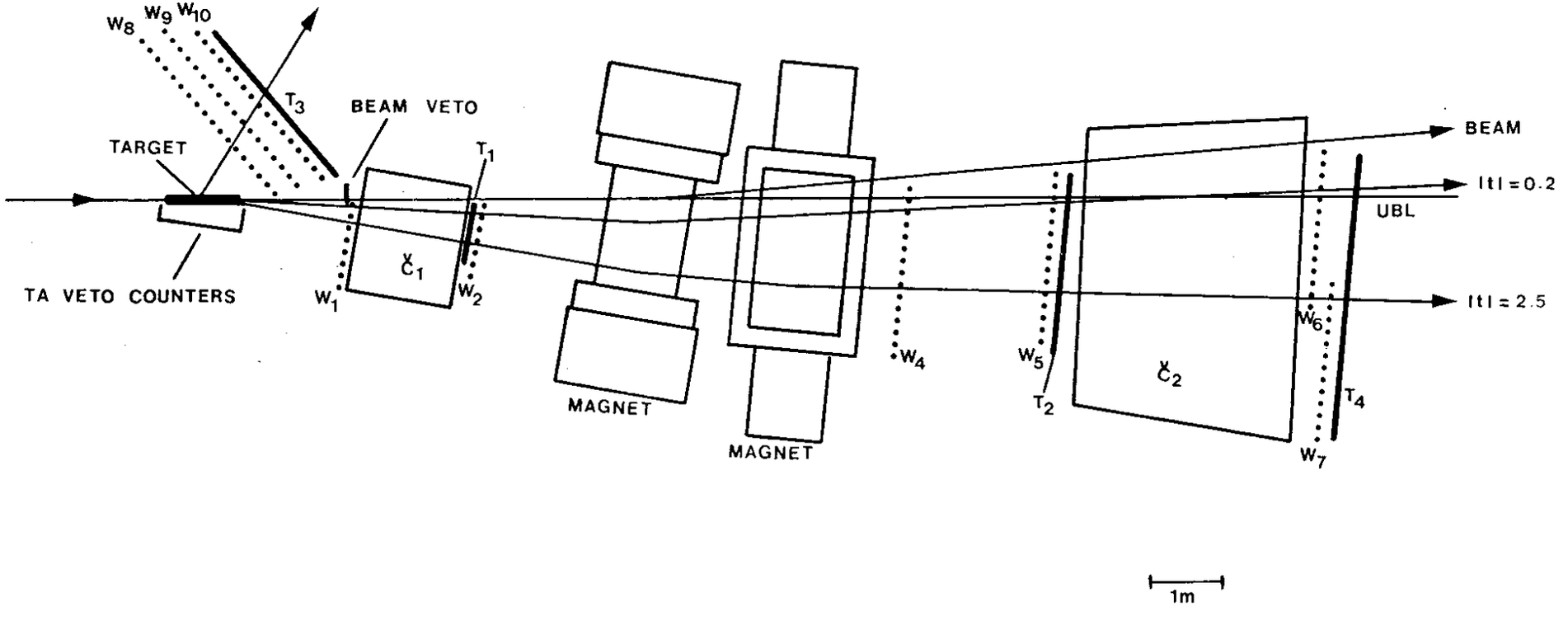

Fig. 5 Layout of the spectrometer for the large angle geometry (geometry 2). C_1, and C_2 are threshold Cerenkov counters. T_1, T_2, T_3, and T_4 are scintillation counter arrays. W_1 to W_{10} are modules of spark-chambers. A few particle trajectories are indicated.

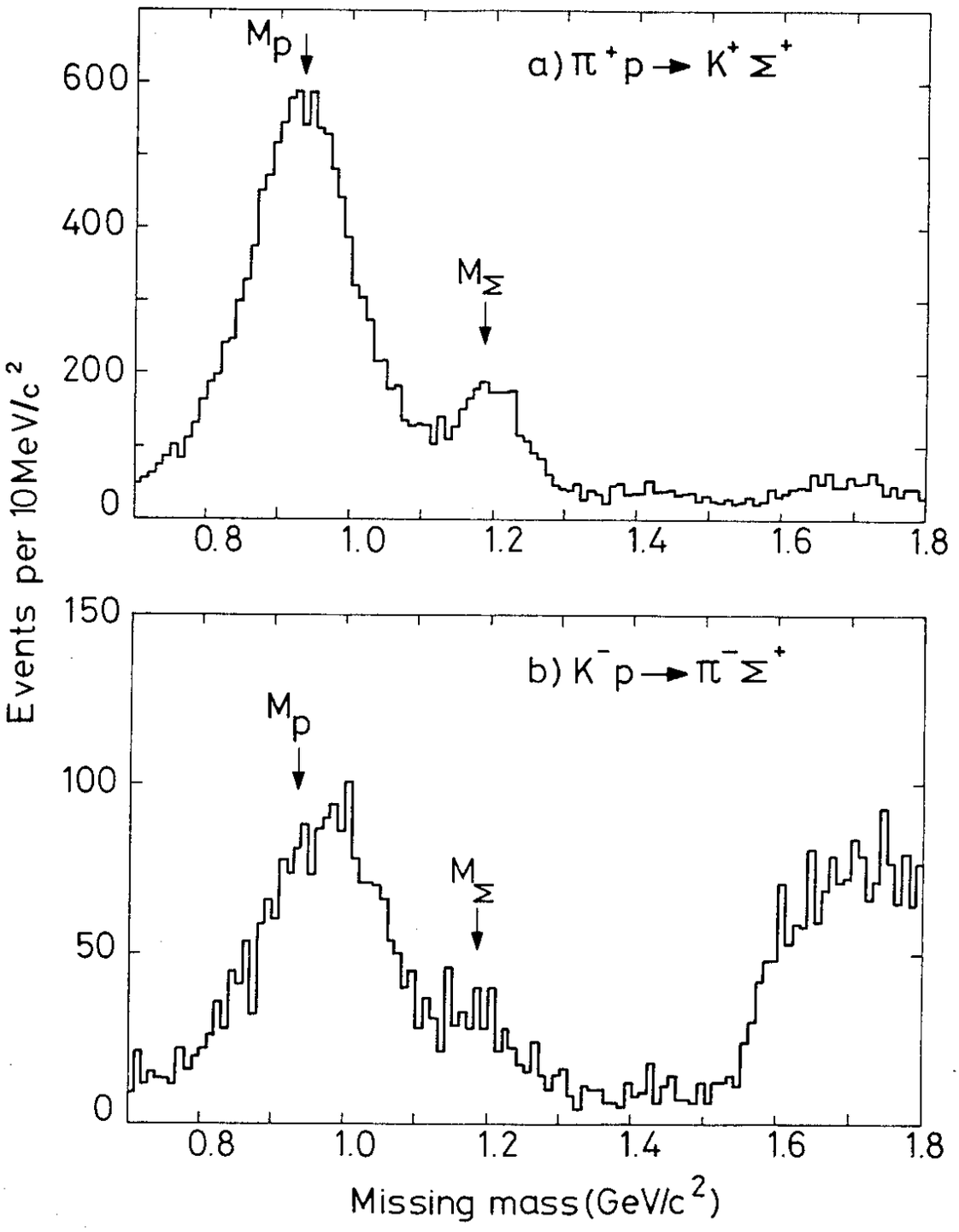

Fig. 6 Missing mass distributions for a sample of the 10.1 GeV/c geometry 1 data. a) and b) show the distributions before any cuts were made.

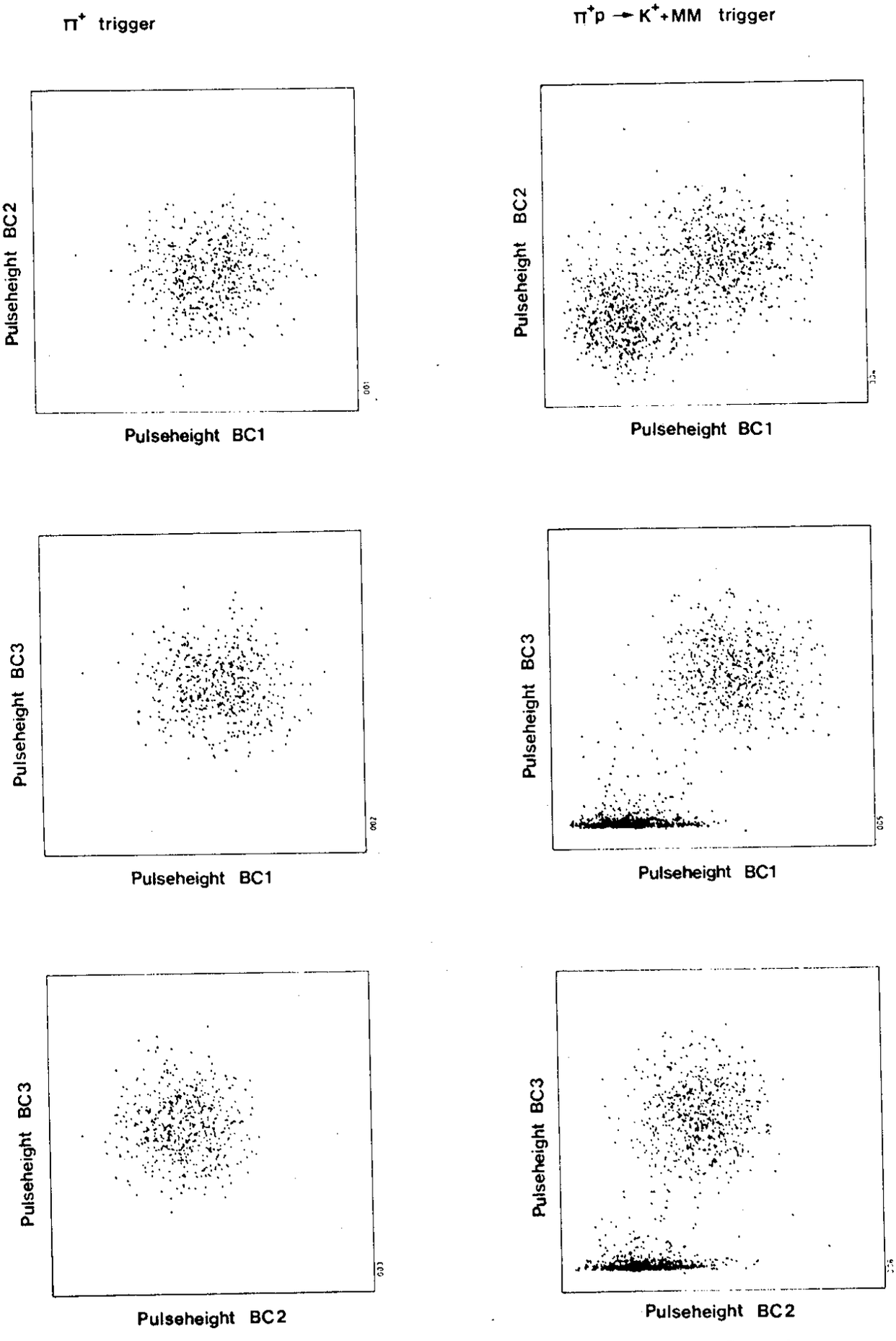

Fig. 7 A scatter plot of pulse heights in the beam Cerenkov counters for pion triggers and $\pi^+p \to K^+$ MM triggers. Note the events with low pulse heights in BC3.

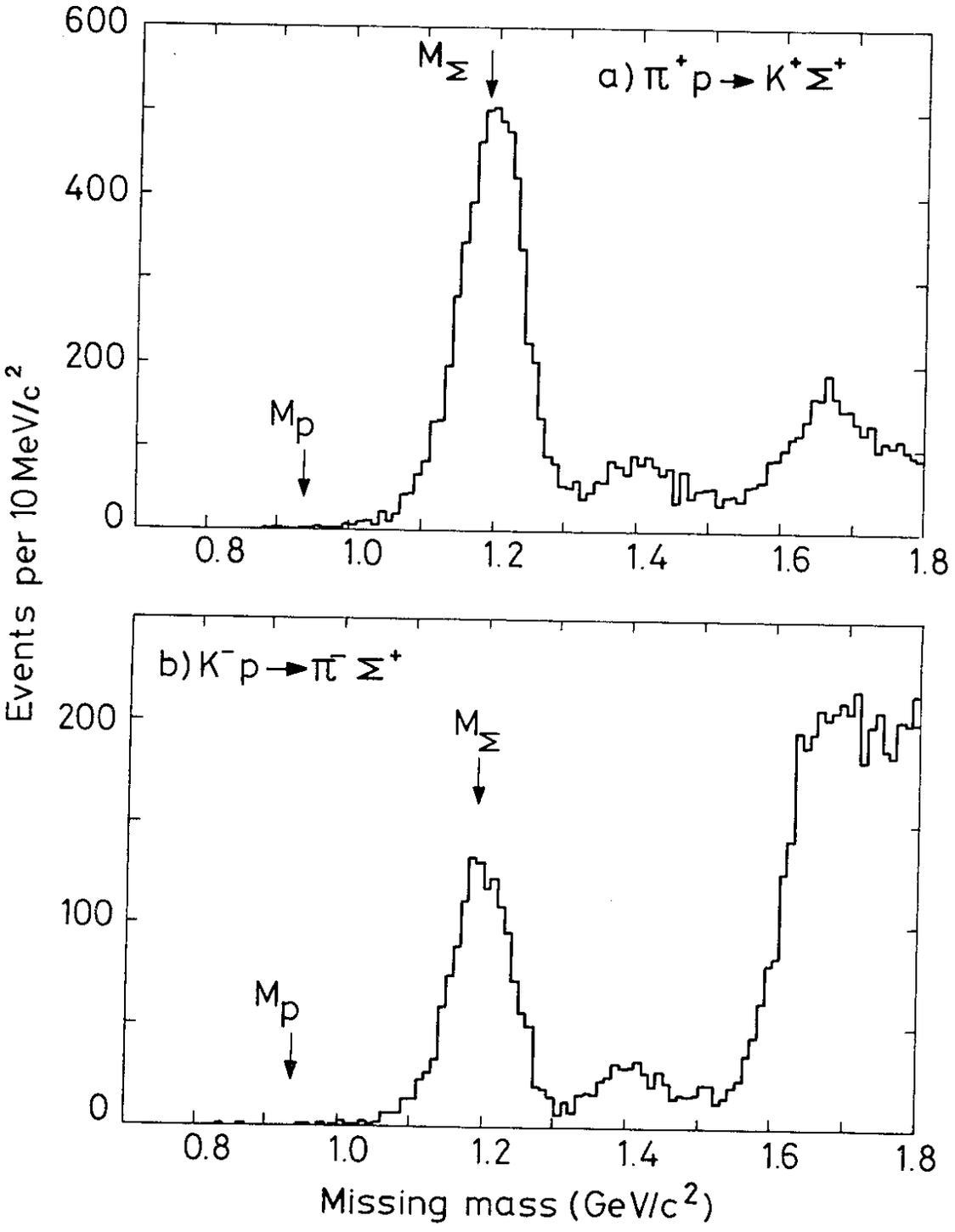

Fig. 8 Missing mass distributions for the 10.1 GeV/c geometry 1 data. a) and b) show the distributions after all the cuts described in the text had been made. The large background above 1.5 GeV/c^2 for the K^- induced reaction arises from the decay $K^- \rightarrow \pi^- \pi^0$. When interpreted as $K^- p \rightarrow \pi^- X$, the resulting missing mass distribution has a threshold at 1.57 GeV/c^2 and is thus irrelevant for the reactions studied in this experiment.

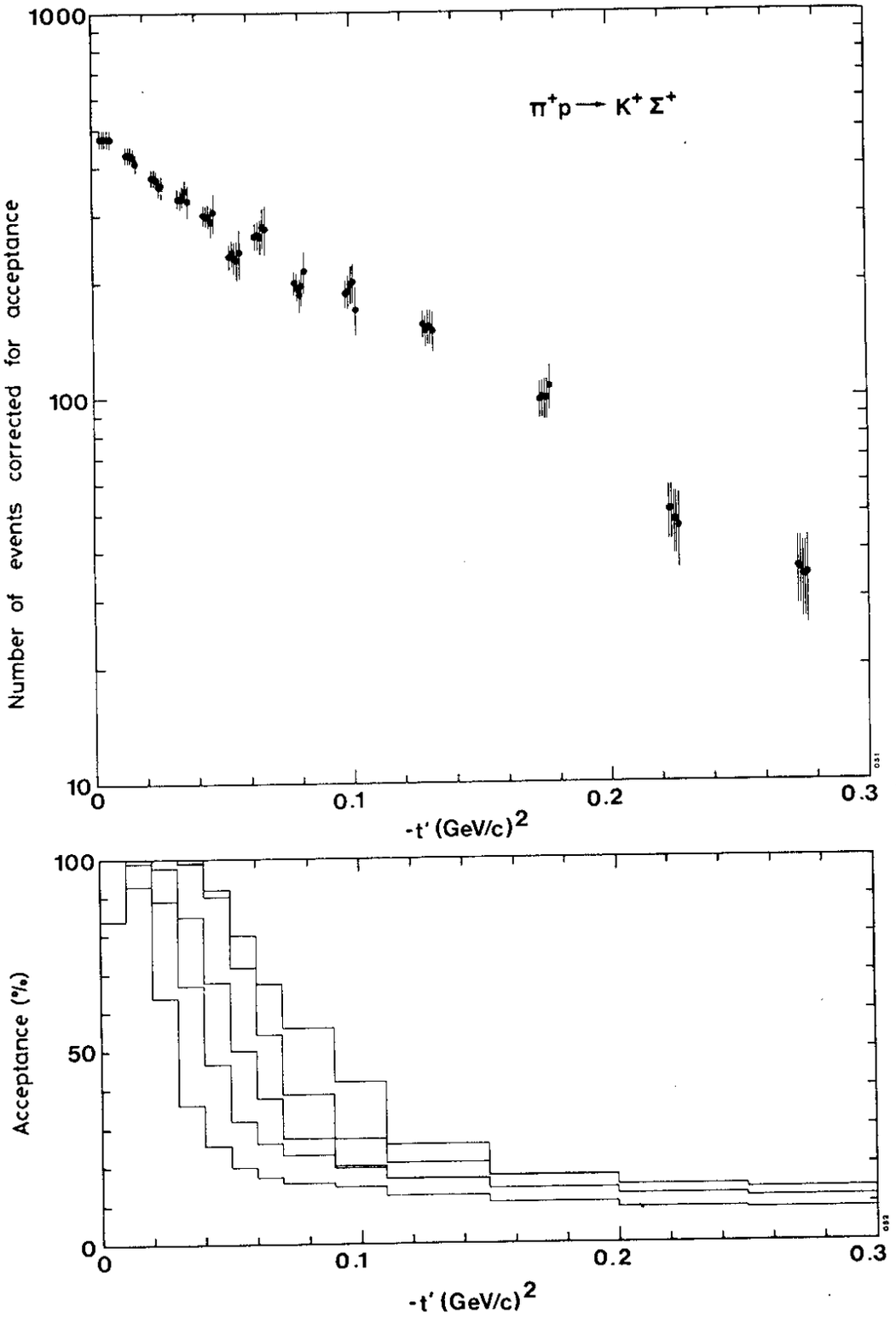

Fig. 9 The results of a test in which the geometrical aperture was decreased by cuts in the analysis program and in the Monte-Carlo acceptance program and the resulting (unnormalized) differential cross-sections. (Note that in each group of five only the centre point is plotted at the correct t' value. The others are displaced slightly for clarity)

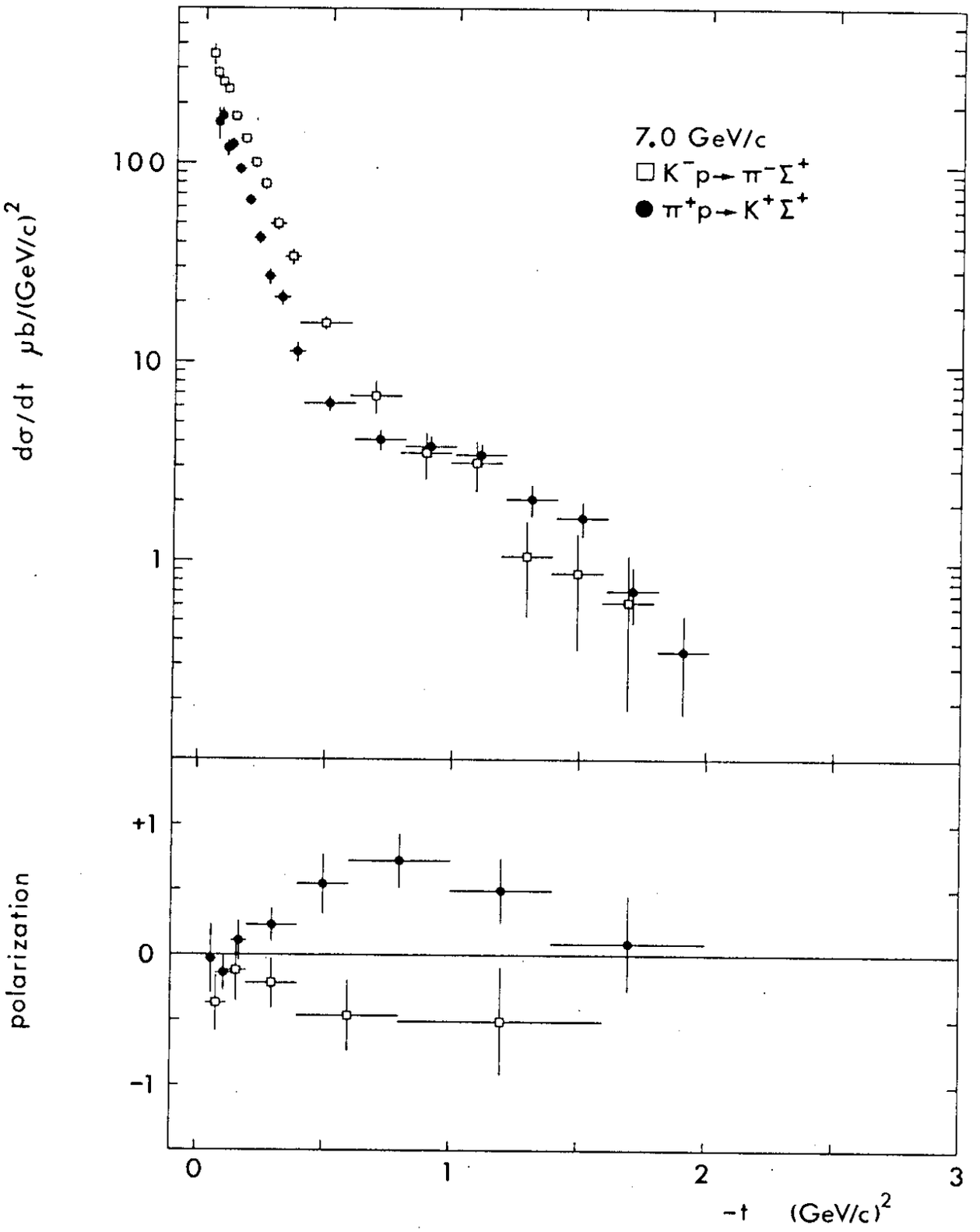

Fig. 10 Differential cross-sections and polarizations for the 7.0 GeV/c data. The filled circles represent $\pi^+p\to K^+\Sigma^+$ and the open squares $K^-p\to\pi^-\Sigma^+$.

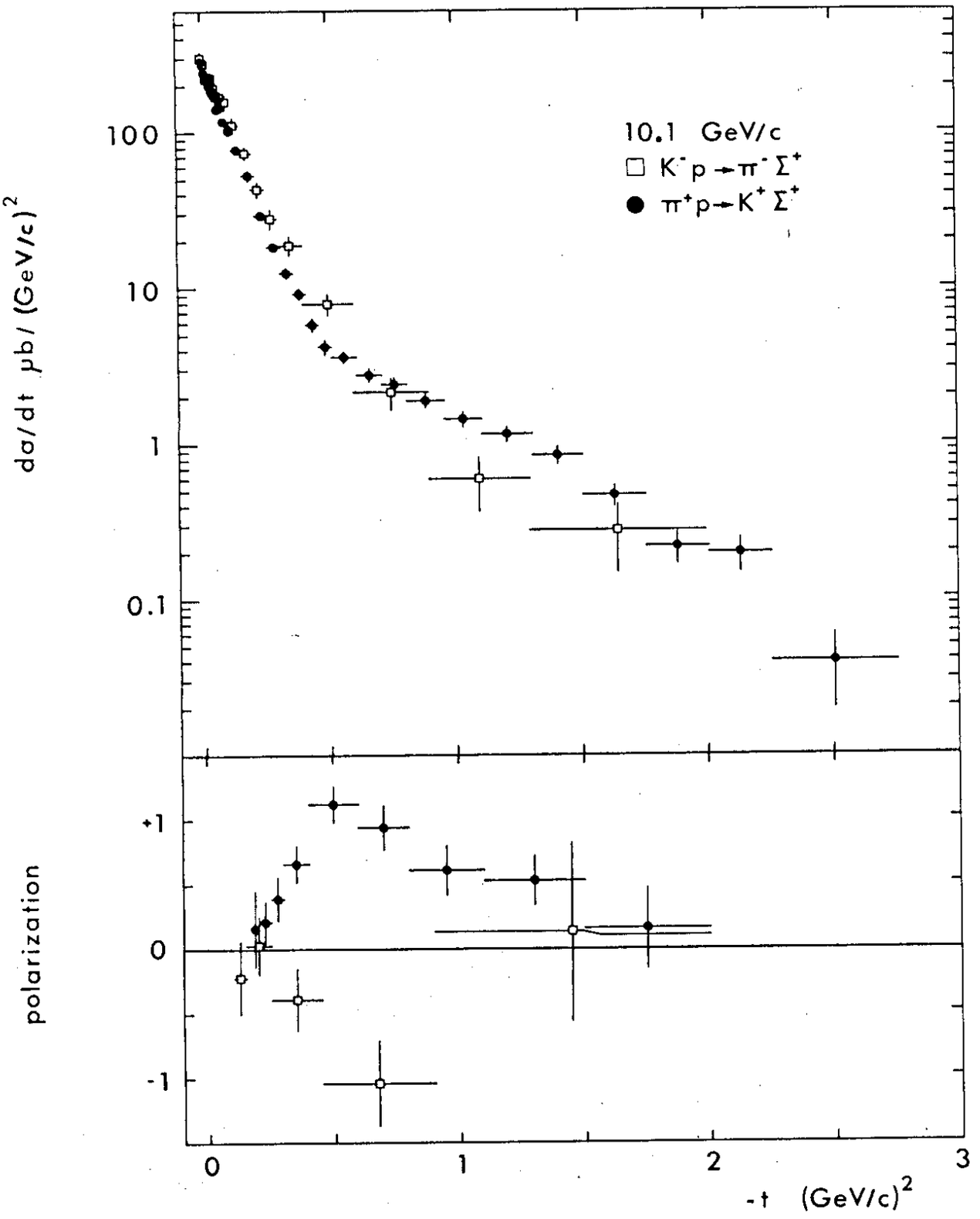

Fig. 11 Differential cross-sections and polarizations for the 10.1 GeV/c data. The filled circles represent $\pi^+p \to K^+\Sigma^+$ and the open squares $K^-p \to \pi^-\Sigma^+$.

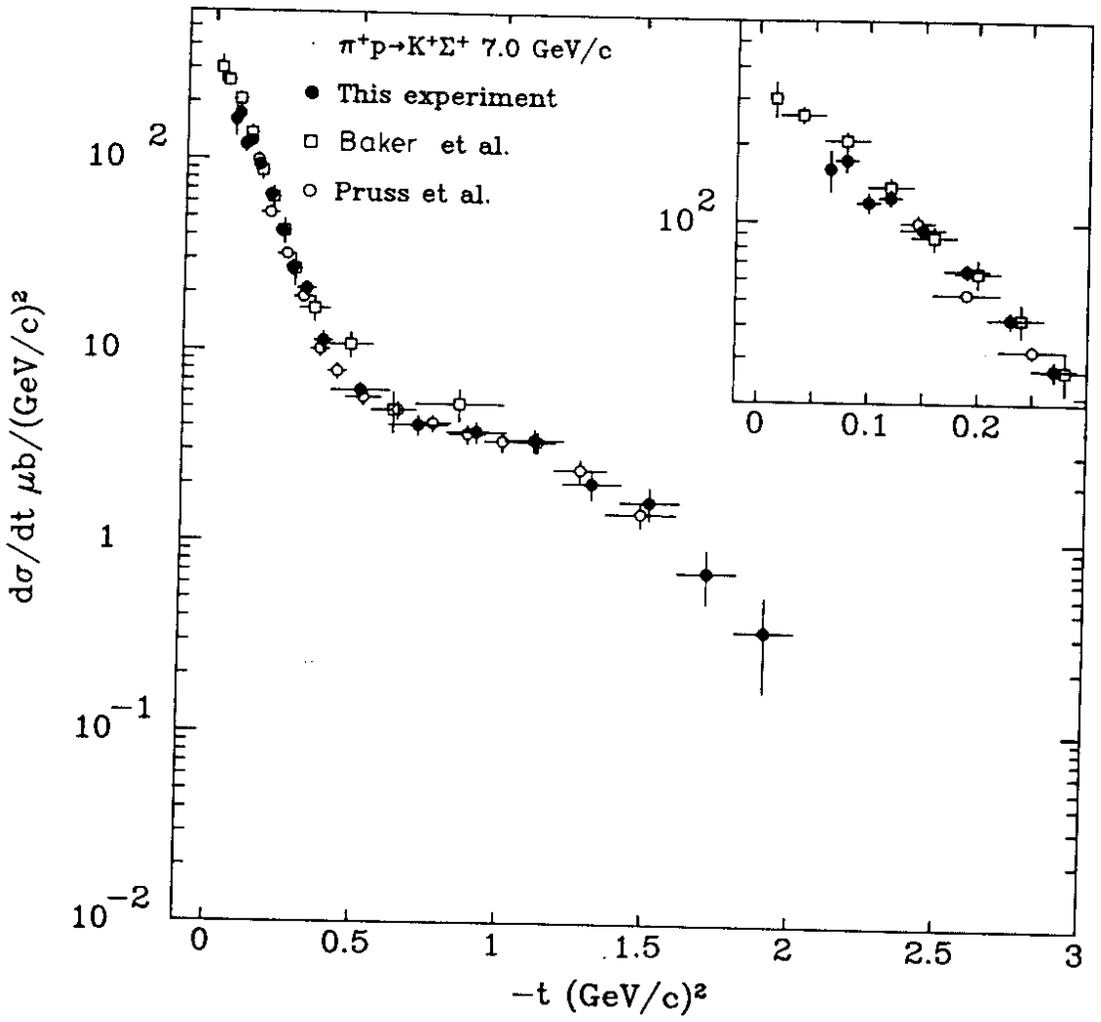

Fig. 12 Comparison between the present measurements and those of Pruss et al. [11] and Baker et al. [12] for reaction (1) at 7.0 GeV/c. The insert shows the region $|t|<0.3$ (GeV/c)^2 in greater detail.

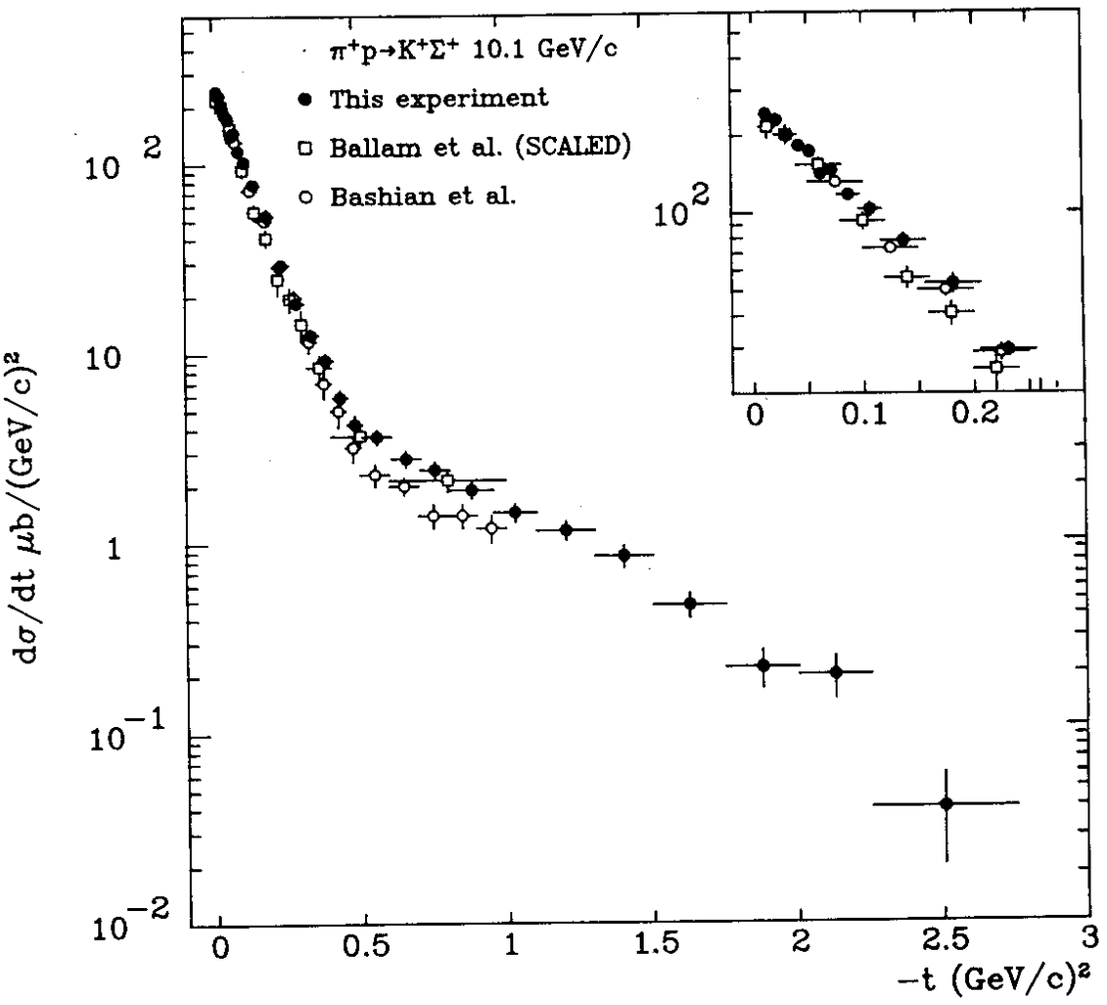

Fig. 13 Comparison between the present measurements and those of Bashian et al. [13] and Ballam et al. [14] for reaction (1) at 10.1 GeV/c. The latter data have been scaled from 11.5 GeV/c

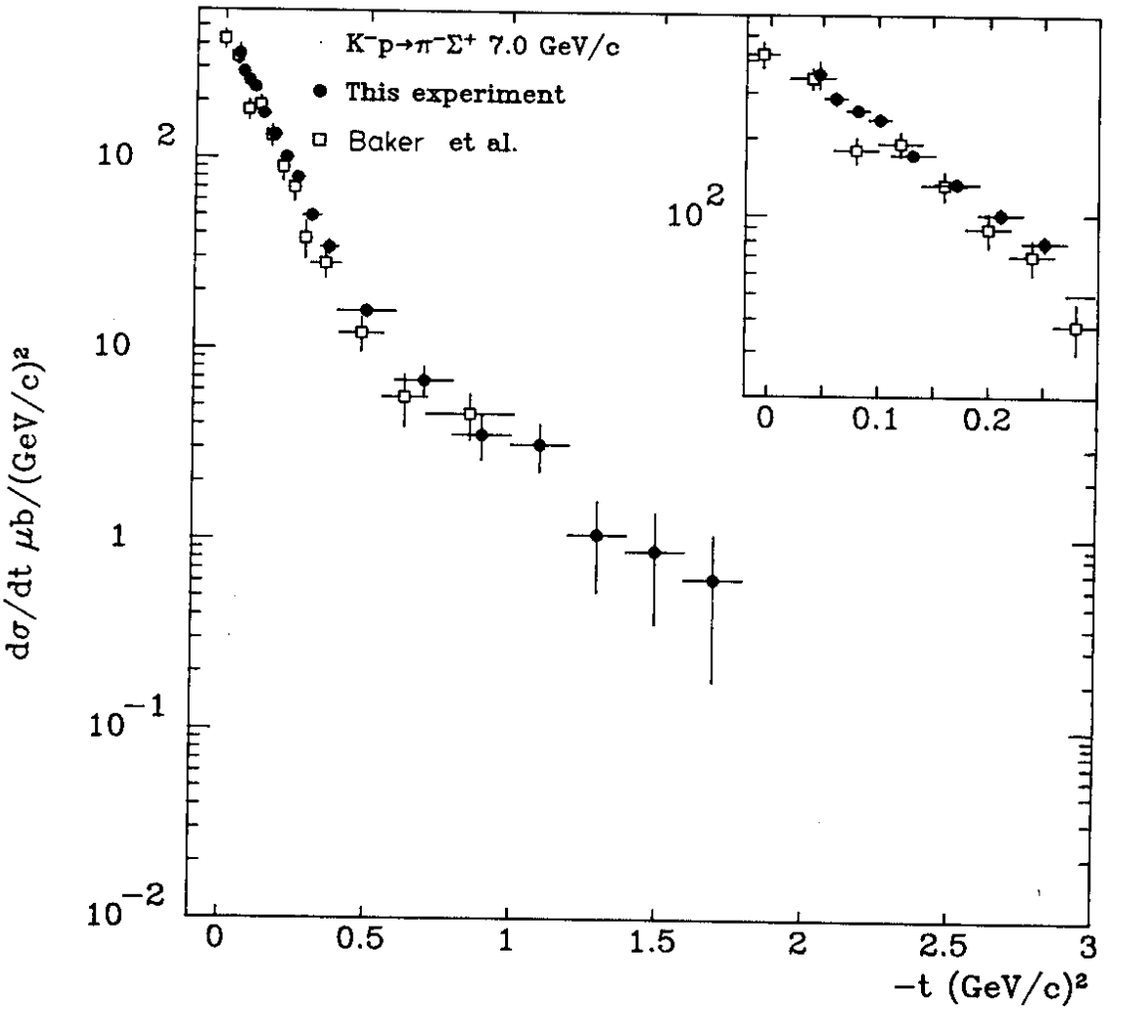

Fig. 14 Comparison between the present measurements and those of Baker et al. [12] for reaction (2) at 7.0 GeV/c. The insert shows the region $|t|<0.3$ (GeV/c)^2 in greater detail.

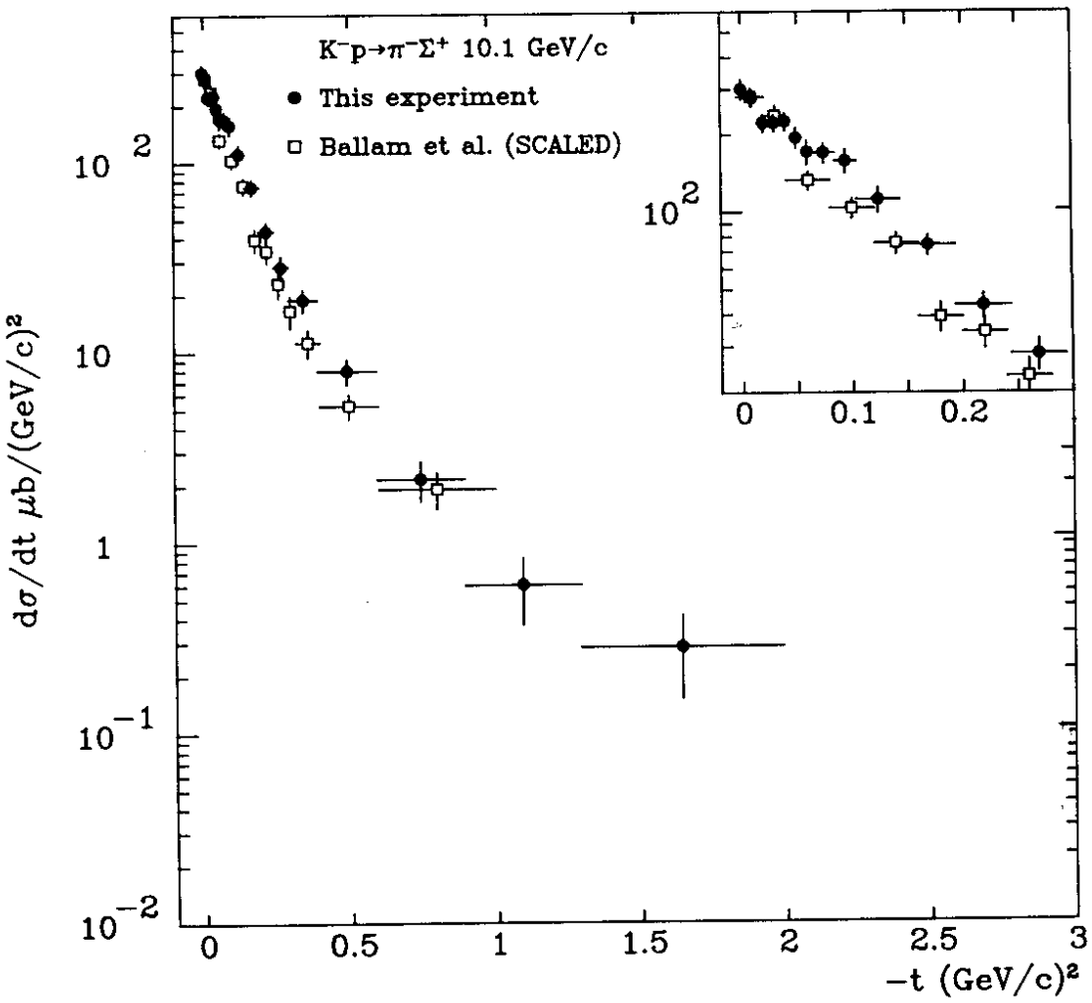

Fig. 15 Comparison between the present measurements and those of Ballam et al. [14] for reaction (2) at 10.1 GeV/c. The latter data have been scaled from 11.5 GeV/c.

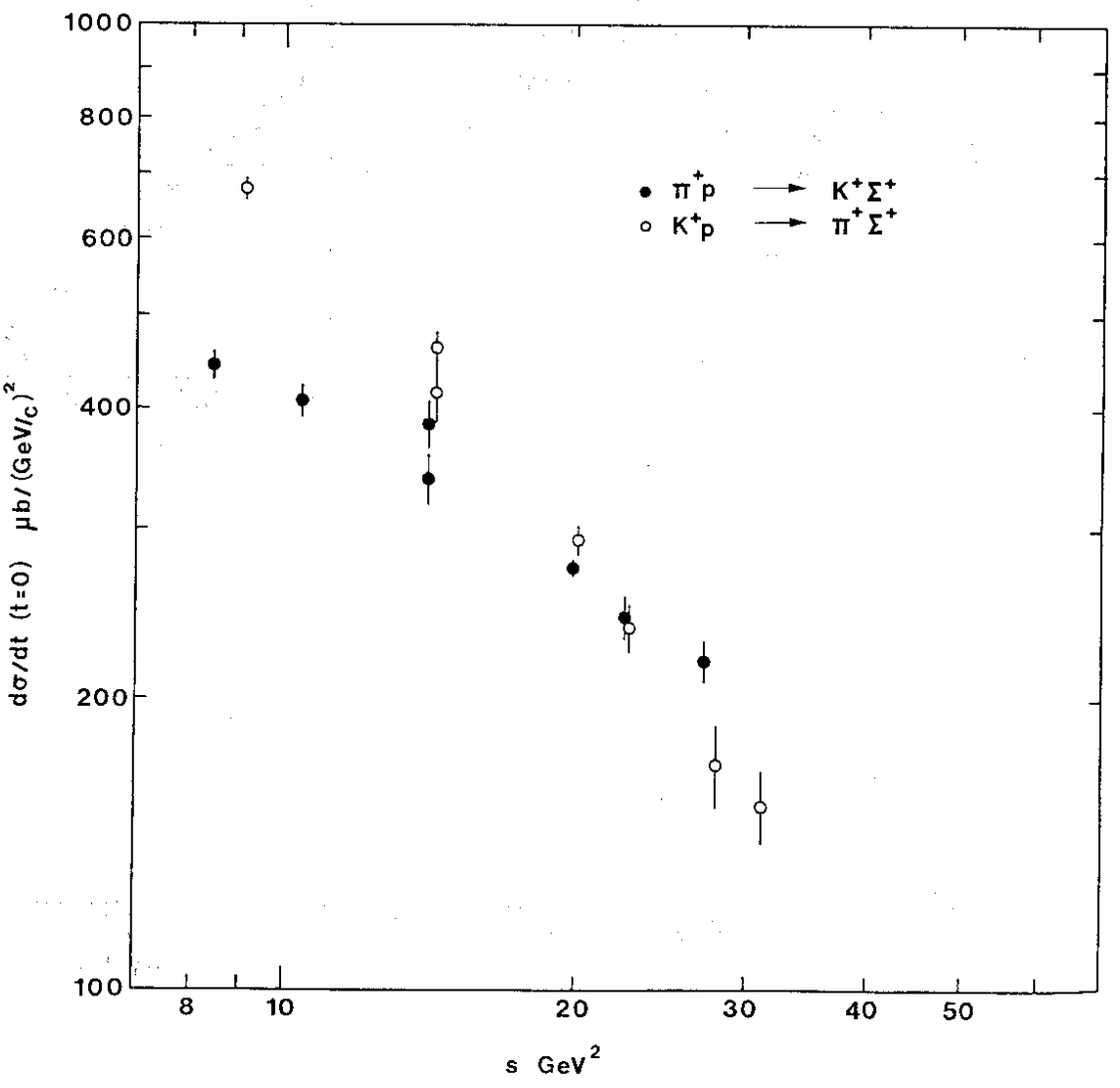

Fig. 16 . Differential cross-sections extrapolated to t=0 for $\pi^+p \rightarrow K^+\Sigma^+$ (filled circles) and $K^-p \rightarrow \pi^-\Sigma^+$ (open circles) as a function of s. Data from this experiment and for $\pi^+p \rightarrow K^+\Sigma^+$ from Pruss et al. at 4, 5.05 GeV/c [11], Baker et al. at 7.0 GeV/c [12], Ballam et al. at 11.5 GeV/c [14], and from Bashian et al. at 14 GeV/c [13], for reaction $K^-p \rightarrow \pi^-\Sigma^+$ from Massaro et al. at 4.2 GeV/c [ref. 16], Baker et al. at 7.0 GeV/c [12], Ballam et al. at 11.5 GeV/c [14], and Chaurand et al. at 14.3 GeV/c [17] and from Birnbaum et al. at 16 GeV/c [18].

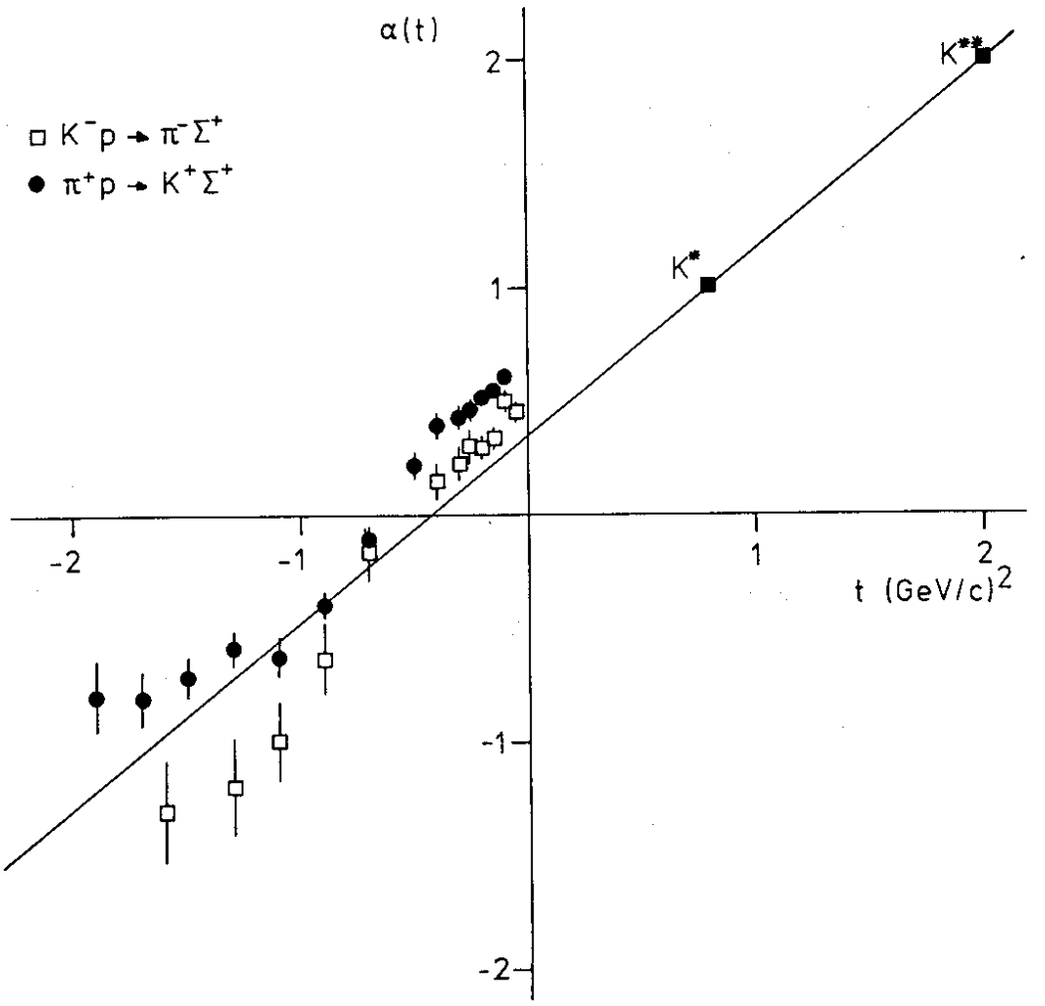

Fig. 17 $\alpha_{eff}(t)$ as a function of t based on the data of this experiment and that of experiments at lower energies (see text).

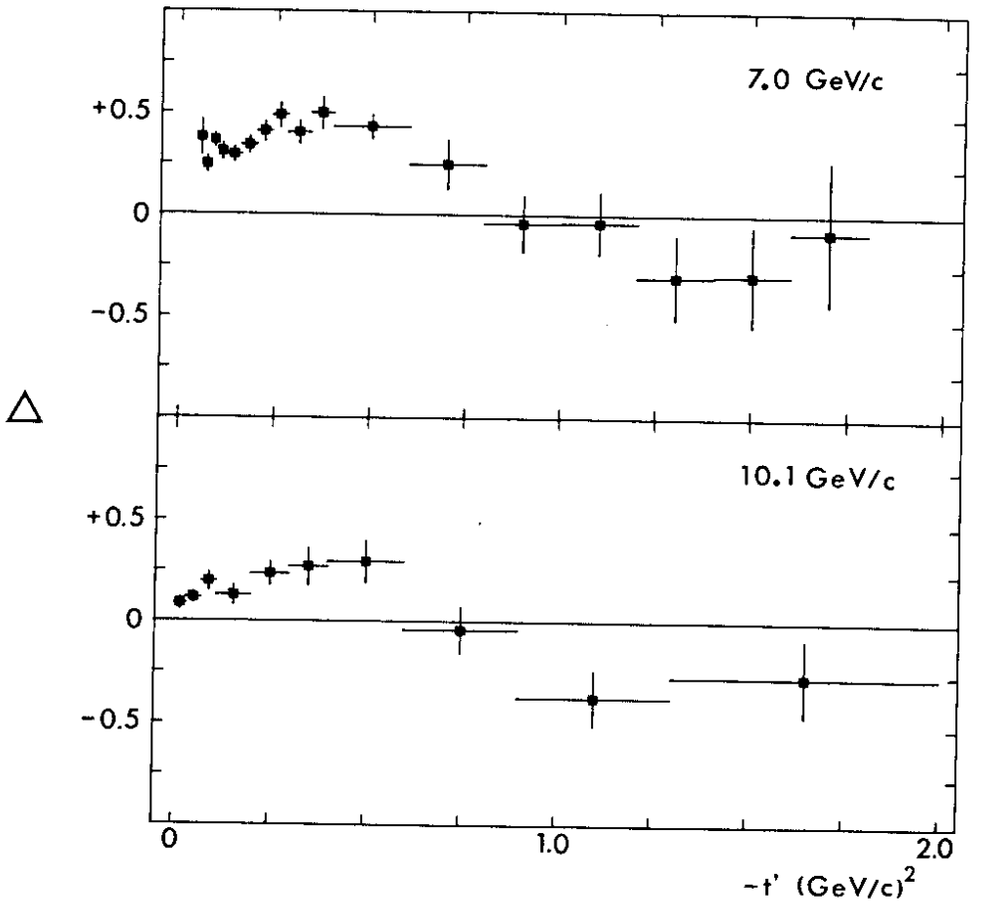

Fig. 18 Normalized cross-section differences, Δ, as a function of t' for the 7.0 GeV/c and 10.1 GeV/c data.

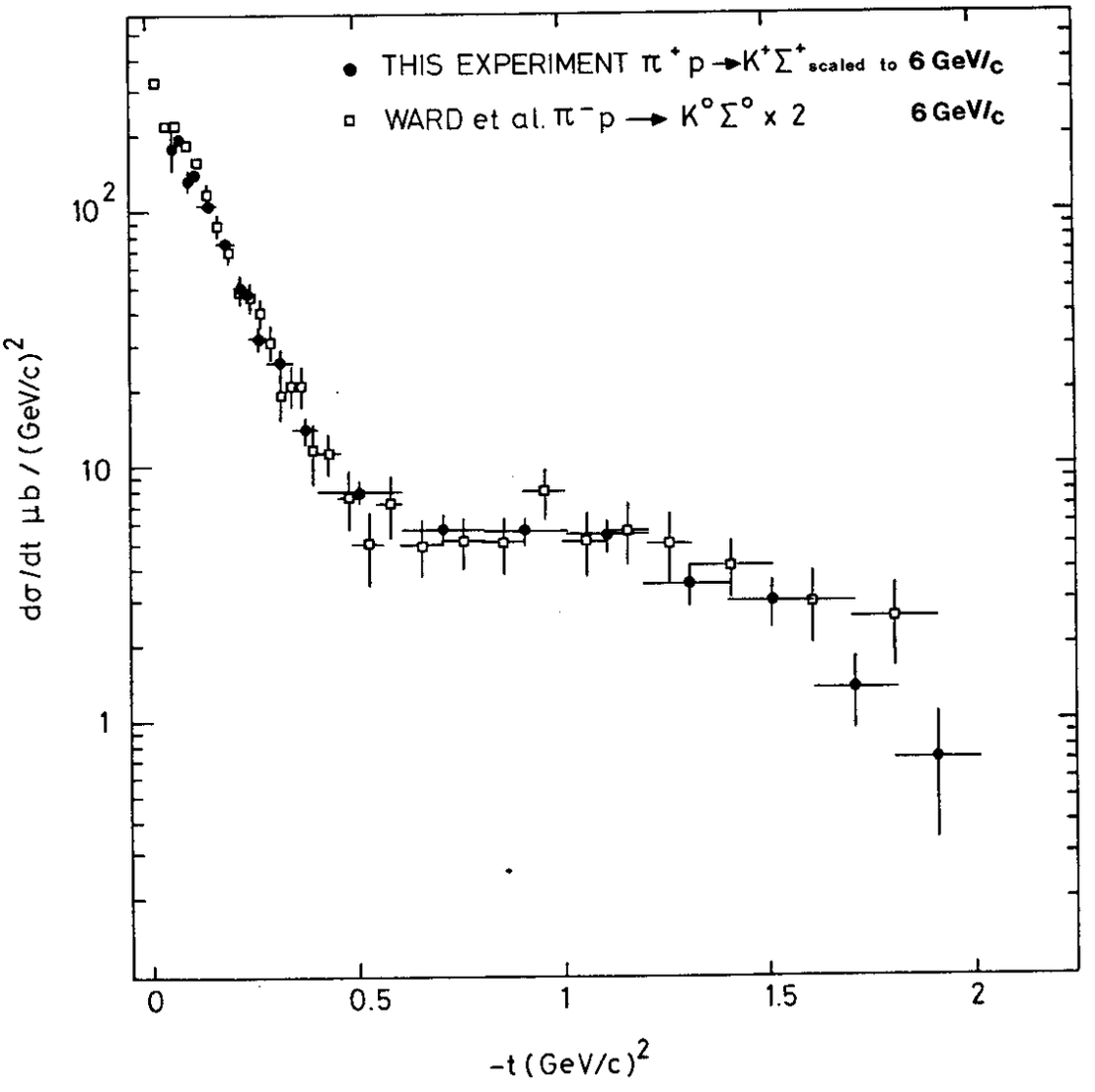

Fig. 19 Comparison between the reactions $\pi^+p \to K^+\Sigma^+$ (data from this experimentat 7 GeV/c, scaled to 6 GeV/c) and $\pi^-p \to K^0\Sigma^0$ at 6.0 GeV/c [19] confirming the dominance of the I=1/2 exchange.

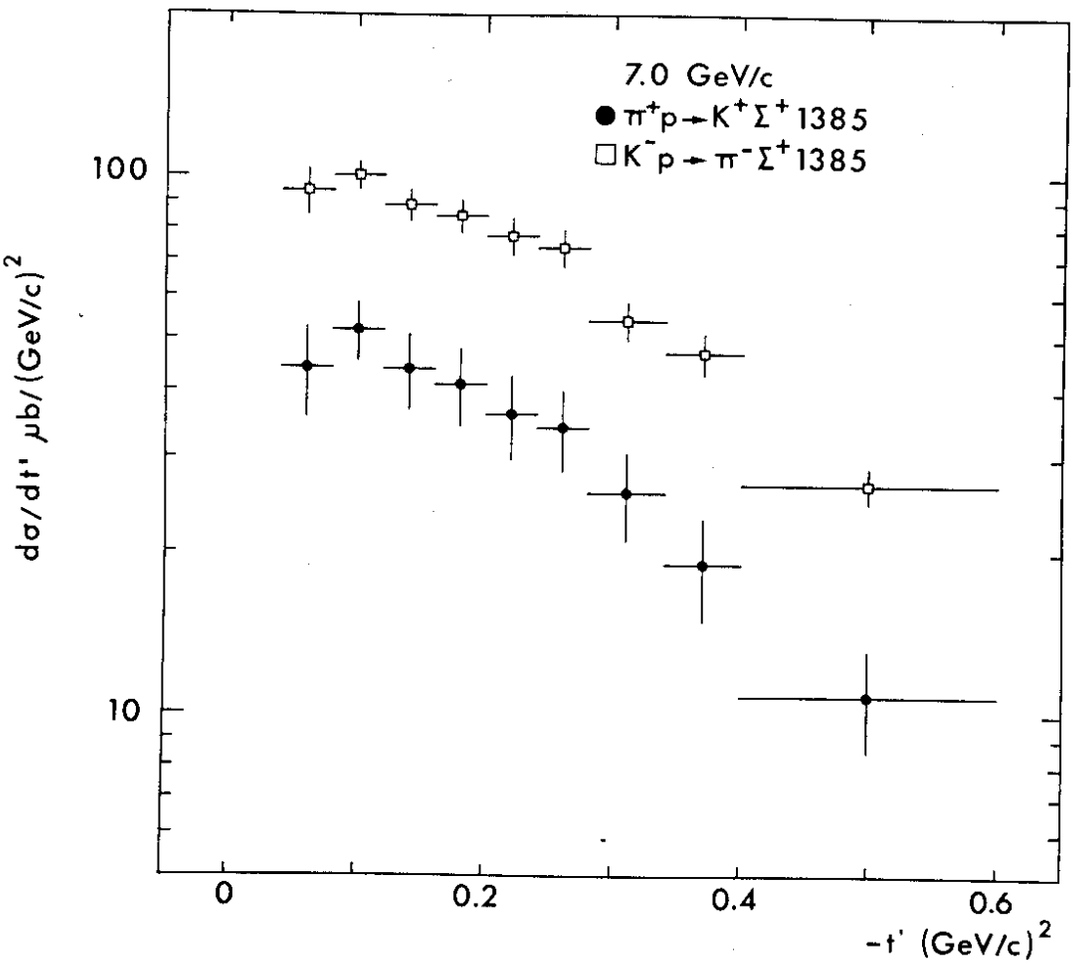

Fig. 20 Differential cross-sections for $\Sigma^+(1385)$ production at 7 GeV/c, measured in this experiment. Circles are $\pi^+p \to K^+\Sigma^+(1385)$ and open squares $K^-p \to \pi^-\Sigma^+(1385)$.

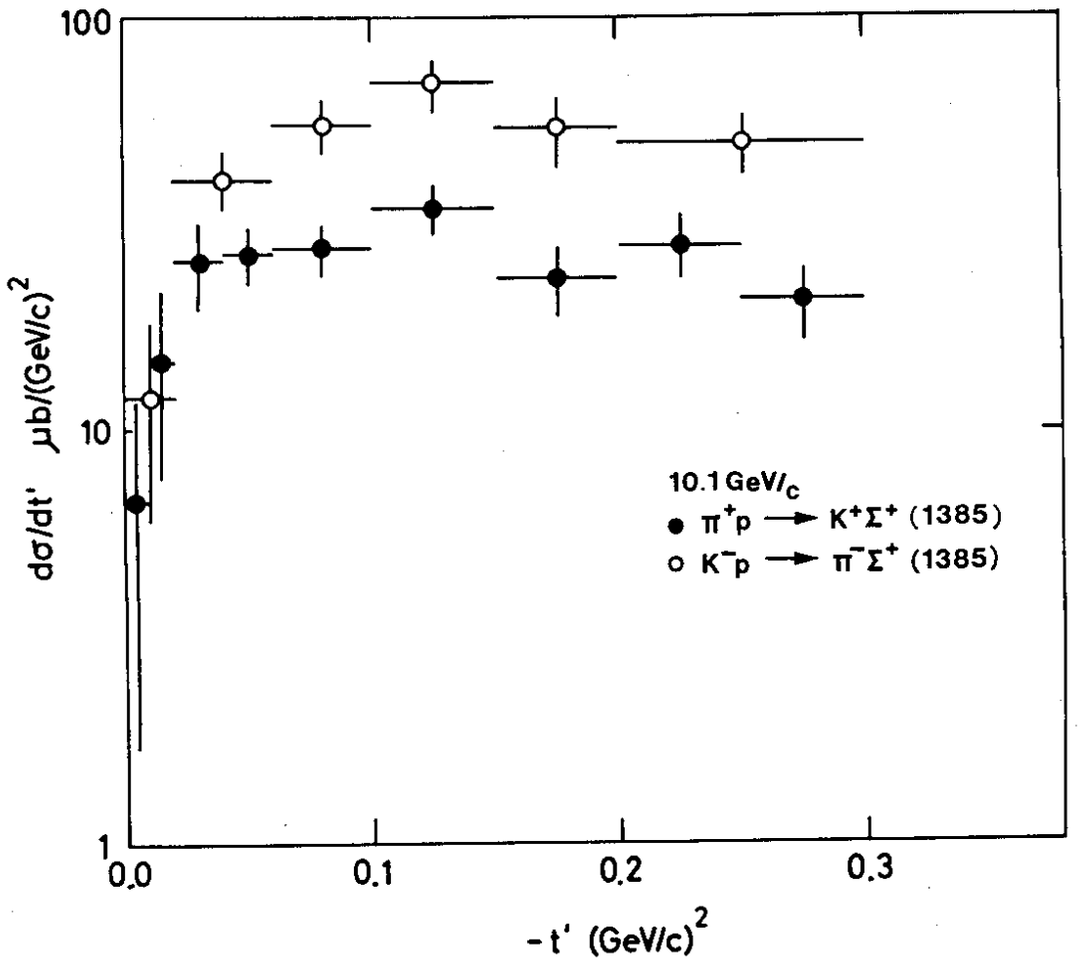

Fig. 21 Differential cross-sections for $\Sigma^+(1385)$ production at 10.1 GeV/c, measured in this experiment. Circles are $\pi^+p \to K^+\Sigma^+(1385)$ and open circles $K^-p \to \pi^-\Sigma^+(1385)$.

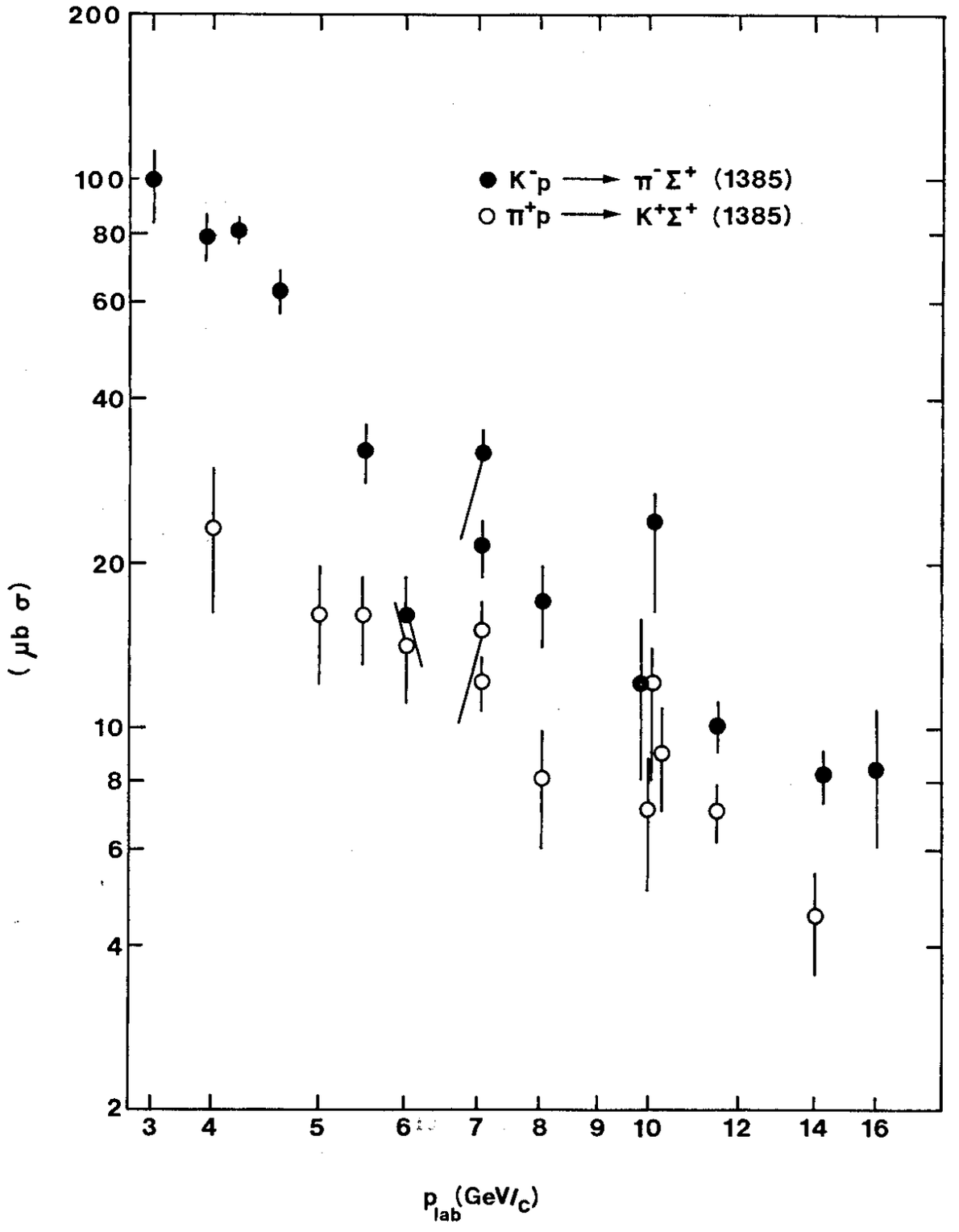

Fig. 22 Compilation of Σ(1385) cross-sections plotted as a function of beam momentum ([13, 17, 18, 21, 22, 23, 24, 25, 26]).

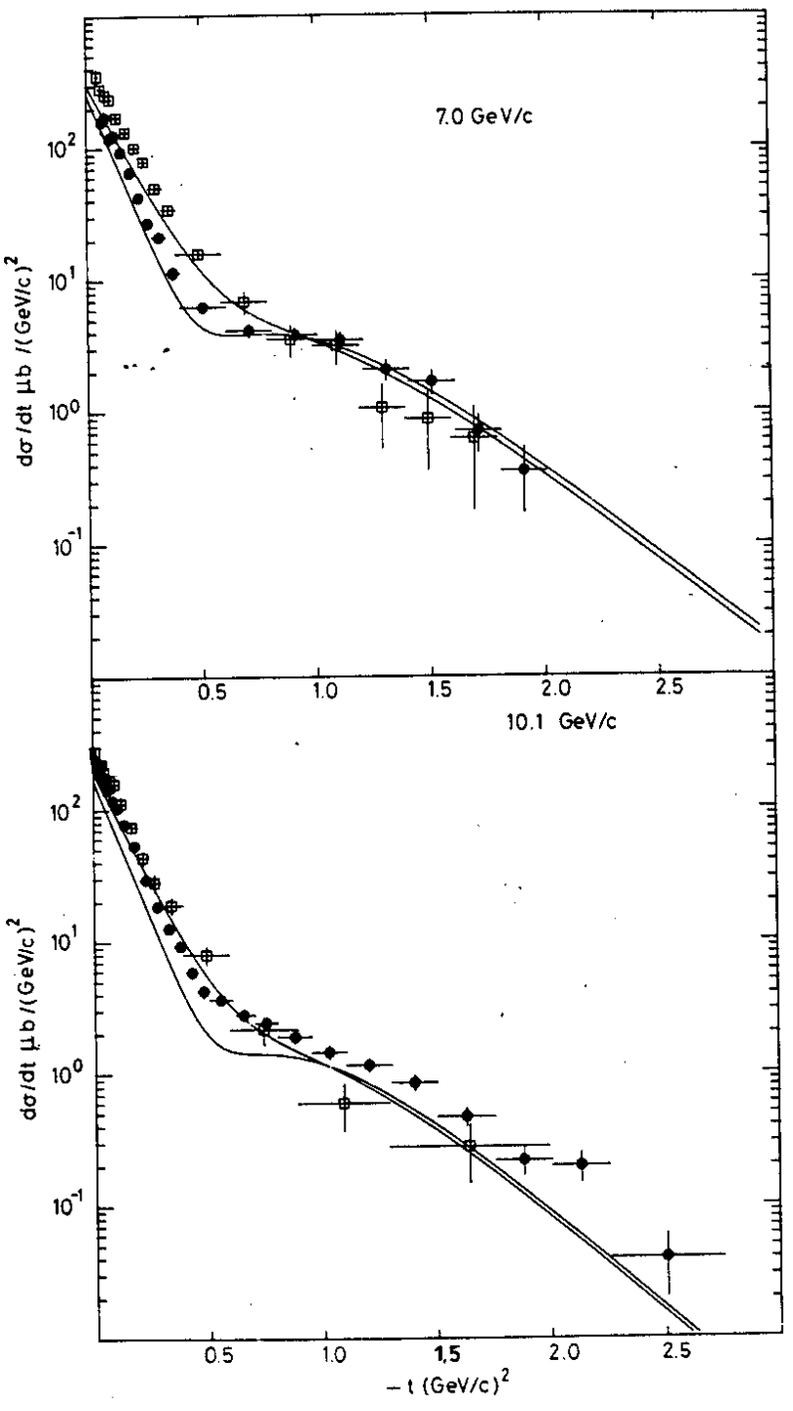

Fig. 23 The differential cross-sections for the reactions $\pi^+p \to K^+\Sigma^+$ (full circles) and $K^-p \to \pi^-\Sigma^+$ (open squares) at 7.0 and 10.1 GeV/c measured in this experiment, compared with the predictions of Navelet and Stevens [35].